International Journal of Earth Sciences (2021) 110:559–582
https://doi.org/10.1007/s00531-020-01971-0

ORIGINAL PAPER

Petrographic and geochemical characterization of the Middle–Upper Jurassic Fe–Mn crusts and mineralizations from Monte Inici (north-western Sicily): genetic implications

Giovanna Scopelliti[1] · **Valeria Russo**[1]

Received: 1 May 2020 / Accepted: 29 November 2020 / Published online: 18 January 2021

Abstract

Fe–Mn concretions and mineralizations, associated with condensed horizons and hardground, are significant archives in ancient carbonate rocks. Their petro-chemical study allows an assessment of the palaeoenvironmental context in which they were formed also connected to their biotic or abiotic origin. At the western side of the Monte Inici (Fornazzo section, north-western Sicily) a well exposed outcrop of condensed pelagic limestones (Rosso Ammonitico facies: Middle−Upper Jurassic) is well-known and thoroughly studied. In this section, the base of the Rosso Ammonitico facies consists of a very condensed level rich in fossils with a variable thickness deposited from the early Bathonian to the early/middle Callovian. It is characterized, at the top, by the noticeable presence of Fe–Mn concretions, typical of the Tethyan Jurassic and related to very low sedimentation rates. For this study, Fe–Mn crusts and mineralizations from the Fornazzo section were investigated using X-ray diffraction, scanning electron microscopy, X-ray fluorescence, ICP and stable-isotope mass spectrometry. The collected samples, deposited in submarine conditions (as testified by stable oxygen and carbon isotopes), have been subdivided in two typologies with different macroscopic and mineralogical features. The Fe–Mn crusts consist of hematite, todorokite and birnessite and are characterized by a relatively low Mn/Fe ratio. Their content in trace elements, rare earths and yttrium (REY) is compatible with a hydrogenetic origin involving the oxy-hydroxides colloids precipitation directly from seawater. Microbially mediated processes are here testified by the recognition of filamentous and coccoid-shaped microstructures referable to coexistence of chemosynthetic fungi and photosynthetic cyanobacteria and accounting for a deposition in the deep euphotic zone. An average growth rate of ~ 8.5 mm/Myr for the Fe–Mn crusts, estimated by cobalt concentrations, suggests a time elapsed for deposition of ~ 3.5 ± 1 Myr. This value is compatible with the stratigraphic gap embracing the time span from the early/middle Callovian to the middle Oxfordian. In the neighbouring pelagic limestones, Fe–Mn deposits are present in the form of micro-dendrites mainly consisting of pyrolusite, sometimes associated with carbonato-fluorapatite. The geochemical composition gives evidence of a prevalent early diagenetic origin with precipitation, at the sediment/water interface or in the first centimeters of sediments, of metals diffused from the crusts as consequence of fluctuating redox conditions. Although the well-preserved *Frutexites* texture is commonly related to a microbial activity, other bacterial microstructures have not been recognized, having probably been obliterated during the growth of the dendrites. Nevertheless, it is possible to suppose a deepening in the bathymetry consistent with the involvement of chemosynthetic microorganisms in the formation of *Frutexites* structures.

Keywords Fe–Mn crusts · Frutexites · Microbial mediation · Mineralogy · Trace elements · REE · Stable isotope · Growth rate

Introduction

The Fe–Mn crusts, nodules and mineralizations, associated to rockground or hardground (sensu Clari et al. 1995) formed in ancient carbonate rocks or in present marine sediments, represent a significant lithofacies indicating peculiar geological and biogeochemical environments (Ehrlich 1975;

Valeria Russo is currently an independent researcher.

✉ Giovanna Scopelliti
giovanna.scopelliti@unipa.it

[1] Dipartimento di Scienze della Terra e del Mare (DiSTeM), Palermo University, Palermo, Italy

Palmer and Wilson 1990; Fürsich et al. 1992; García-Ruiz et al. 1994; Clari et al. 1995; Gupta 1995; Bayon et al. 2004; Reolid 2011; Föllmi 2016; Jiang et al. 2020) and sometimes significant potential metal source (Ehrlich 1975; Rona 2003; Polgári et al. 2004; Hein et al. 2013; Kuhn et al. 2017; Marino et al. 2019). These deposits are characterized by a complex mineralogical and chemical composition, with prevalence of iron and manganese but also showing relatively high concentration of trace elements as Co, Cu, Ni, Cr, V (e.g.,Nicholson et al. 1997; Rona 2008; Hein et al. 2010). They frequently represent "condensed stratigraphic sequences", growing with a very low rate and recording in their structure, texture, mineralogy and geochemistry the oceanic conditions during their growth process (e.g., Koschinsky et al. 1996; O'Nions et al. 1998; Abouchami et al. 1999; Hein et al. 2000; Hlawatsch et al. 2002; Han et al. 2003; Claude et al. 2005).

As for their origin, marine Fe–Mn crusts and mineralizations are generally classified as: hydrogenetic, diagenetic, and hydrothermal (Bolton et al. 1988; Hein et al. 1997; Glasby 2000). The first type is represented by ferromanganese crusts, which slowly precipitate from seawater at the seabed on to hard-rock substrate. Diagenetic deposits result from direct precipitation of Fe–Mn oxy-hydroxides during early diagenesis at or below the seafloor, usually in response of changing redox conditions (Force and Cannon 1988; Hein and Koski 1987; Okita et al. 1988; Jach and Dudek 2005; Guido et al. 2016). Finally, Fe–Mn nodules and/or crusts related to submarine hydrothermal systems precipitate directly from hydrothermal solutions associated to submarine volcanism (Manheim and Lane-Bostwick 1988; Fleet 1993; Abad et al. 2010; Marino et al. 2019). In addition to these three main typologies, or rather, interplaying with them in particular conditions, processes of biomineralization have been added (Lin et al. 1996; Han et al. 1997; Wang et al. 2009; Polgári et al. 2012; Lozano and Rossi 2012; Rajabzadeh et al. 2017). Stromatolite-like textures, similar to those found in limestone, are widely documented also in Fe–Mn nodules and crusts and are ascribed to biological mediation by either algae (stromatolites) or bacteria (deep water thrombolites) (Jansa et al. 1989; Mamet and Préat 2006a; Polgári et al. 2012; Lozano and Rossi 2012). Unlike the well-defined microbial biosignature in the carbonate fossil record (e.g., Riding 2000), non-carbonate microstructures hardly preserve clear evidence of the organisms possibly responsible for their formation. Among these, *Frutexites* have been linked to microbial processes but their origin and distribution in sedimentary environment are still matter of discussion. The term *Frutexites arboriformis* was firstly used by Maslov (1960) from the name of the homonymous genus including five different species. The identification and description of the fossil *Frutexites* in the literature are always based on: similarity with pelagic stromatolites, dendritic structures mainly composed of iron and/or manganese oxides, several tens to hundreds of micrometers in height. Although a clear relation of these structures to a microbial precursor is today controversial, recently Heim et al. (2017) observed structures strongly resembling the dendritic pattern of fossil *Frutexites* in living iron oxide precipitating biofilms and growing on rock surfaces sampled at 160 m depth in the Äspö Hard Rock Laboratory (Sweden). Indeed, similar microbial microstructures were not only described in marine environments such as shallow and deep water stromatolites, microbial limestones, hardgrounds, condensed pelagic limestones, but also in continental setting like veins and fractures of deep subterranean environments (Rodríguez-Martínez et al. 2011 and references therein).

Among all these environments, the condensed pelagic limestones and hardgrounds from Devonian up to Jurassic remain the last most extended occurrence of Fe–Mn concretions and *Frutexites*. In western Sicily, fossil ferromanganese crusts, nodules and pavements are associated with the base of the condensed pelagic red limestone of the Rosso Ammonitico facies. While an extensive bibliography is available on the biostratigraphy and sedimentology of this condensed pelagic facies as well as regarding the definition of the detailed microfacies (e.g., Gemmellaro 1872–1882; Floridia 1931; Christ 1960; Wendt 1963, 1969; Jenkyns 1970a; Catalano et al. 1981a; Cecca et al. 1992, 2001; Di Stefano 2002; Martire and Pavia 2002; Pavia et al. 2004; Beccaro 2007; Cecca and Savary 2007), only a smaller amount of the papers focus on the petro-geochemical features of the associated Fe–Mn mineralizations. A first review and documentations of their occurrences from this point of view was provided by Jenkyns (1967), but in the following years, with the exception of some papers (Jenkyns 1970b; Di Stefano and Mindszenty 2000; Préat et al. 2011), Sicilian Jurassic Fe–Mn concretions have received little attention in relation to their true origin and significance.

The present study focuses on the petrographic and geochemical characterization of the Fe–Mn crusts and mineralizations included in the exceptionally well-exposed succession of the Fornazzo quarry (Monte Inici, western Sicily). This section has been detailed studied from the biostratigraphic point of view since the 1960s (Wendt 1963) and more recently from Martire and Pavia (2002) and has been proposed by Pavia et al. (2004) for the basal G.S.S.P. boundary of the Tithonian stage identified inside the upper member of the Rosso Ammonitico facies, but despite the well-defined stratigraphic context, the petro-geochemical description and interpretation of the Fe–Mn deposits characterizing the base of the pelagic nodular-calcareous lithofacies, is still missing.

The major goal of this paper is to define the origin of Fe–Mn crusts and mineralizations, discriminating whether their formation was the consequence of the rift-related volcanism (hydrothermal origin) or was mainly related to

hydrogenetic or diagenetic processes. To this purpose, in addition to the major and trace elements, rare earth elements and Y were investigated, because they are recognized as robust tools discriminating the Fe–Mn oxy-hydroxides genesis. Other objectives are (i) to estimate the time span in which the crusts deposited with the aim to better define the stratigraphic gap they are the expression and (ii) to contribute, also by means of petrographic observations, to the scientific debate on the biotic or abiotic origin of these peculiar deposits, also to better define the palaeonvironmental conditions of their deposition.

Geological setting

The studied interval outcrops in the disused Rosso Ammonitico quarry ("contrada Fornazzo") located on the north-western slope of Monte Inici, about 3 km south-westwards of Castellammare del Golfo, in western Sicily (Italy; Fig. 1a, b and e). Monte Inici belongs to a major structural unit of the intermediate zone of the Sicilian–Maghrebian chain (Fig. 1b). This unit derives from the Neogene deformation of a wide palaeogeographic domain pertaining to the African passive margin, known as the Trapanese Domain (Catalano et al. 1996). The stratigraphic record of the Middle and Upper Jurassic in the western Tethys is characterized by common eustatic and tectonic events recorded as stratigraphic unconformities, represented by rockground, hardgrounds, paleokarsts, palaeosoils and the deposition of Fe–Mn crusts and nodules. These latter are formed near the continental margin on seamounts during high sea-level and are characteristic for the Jurassic period in Sicily and other parts of the Tethys region (e.g., Jenkyns 1970b, 1971; Fürsich 1979; Jimenez Espinosa et al. 1997; Di Stefano and Mindszenty 2000).

The "Trapanese type" succession (Fig. 1c), well exposed in the composite Fornazzo section, is characterized by several thousand meters of Upper Triassic peritidal dolostones, followed upwards by the Lower Liassic peritidal and open-shelf limestones of the Inici Formation (Fm). The age of the topmost deposits of the Inici Fm is generally dated as latest Sinemurian (Gugeberger 1936; Arkell 1956; Giacometti and Ronchi 2000). A Pliensbachian age for the Inici Fm top is reported from Monte Erice and "Rocca chi Parra" (Wendt 1969). In some structural highs (e.g., Monte Kumeta) an anomalous benthic production occurred during early Pliensbachian (Giacometti and Rocchi 2000; Di Stefano 2002). From this time, an intense tectonic activity caused the drastic drop in the carbonate productivity and the drowning of the platform which turned into a complex system of small basins, swells and tilted block slopes. The Inici Fm ends with a widespread depositional unconformity, whose origin has been object of a controversial debate since the 1960s (Wendt 2017 and reference therein). On this compound surface the deposition of condensed and composite pelagic facies associations, informally indicated as Rosso Ammonitico (Catalano et al. 1981b) and equivalent to the Buccheri Fm (Patacca et al. 1979), took place. A main Fe–Mn-encrusted rockground capping the Inici Fm, together with repeated satellite crusts in the above condensed pelagic carbonates, mark this passage (e.g.,Wendt 1963; Jenkyns 1970b; Di Stefano and Mindszenty 2000; Di Stefano et al. 2002; Préat et al. 2011). In the Fornazzo quarry, the top of the Inici Fm corresponds to a flat surface with clear evidence of erosion on which lies a 10–30 cm thick and very condensed level described in detail as "level 1" by Martire and Pavia (2002) (Fig. 1d, f). This condensed, discontinuous and rich in fossils level, were made famous by Wendt (1963), who reported a long list of ammonites describing a very rich fossil assemblage, with more than 50 taxa with forms spanning from the early Bathonian to the early and even the middle Callovian. A Fe–Mn encrusted bed, constituting the floor of the quarry, coats the top of the "level 1" with a variable thickness from 0.1 to 8 cm and is the subject of this study (Fig. 1e, f). These concretions are often present in the depressions (Martire and Pavia 2002), indicating that erosion truncated the top of the "level 1" following a prolonged non-sedimentation phase during which authigenic minerals grew. The stratigraphic succession follow with three units of Rosso Ammonitico, the lower one (RAI) and the upper one (RAS) are calcareous with a more or less developed nodular structure, while the middle unit (RAM) is characterized by thin and regular bedding and by a siliceous composition.

The "Trapanese type" succession upward follows with the calpionellid cherty calcilutites (Chiaramonte Fm, also known as *Lattimusa*) with nodular texture and a color range from white to pink or to green. Calpionellid suggest a pelagic platform depositional environment and date these deposits to Tithonian-Valanginian age. The "Trapanese type" section close with Early Cretaceous to Eocene pelagic cherty calcilutites and marls (Hybla and Amerillo Fms *Auct.*, also known as *Scaglia*), which hovewer do not outcrop in the studied area (Fig. 1c; Catalano et al. 1996).

Materials and methods

Samples object of this study come from the disused quarry of Rosso Ammonitico quarry, located in "Contrada Fornazzo" on the Monte Inici north-western side (Fig. 1a). In particular, the Fe–Mn crusts represents the quarry floor from which five samples were taken (Fig. 1e, f). Samples, named HI 1–5, have been subsequently sub-sampled on the base of difference in macroscopic features and mineralogical composition in limestone (1a), dendrites in limestone (1b, 2a, 2b, 3a, 3b, 4a) and laminated Fe–Mn crusts (4b, 5a, 5b)


A
Map data ©2020 2 km
San Vito Lo Capo
Zarbo di Mare
Macari
Tonnarella dell'Uzzo
Castelluzzo
Scopello
Trapani
Visicari
SS187
Balata di Baida
Castellammare del Golfo
Buseto Palizzolo

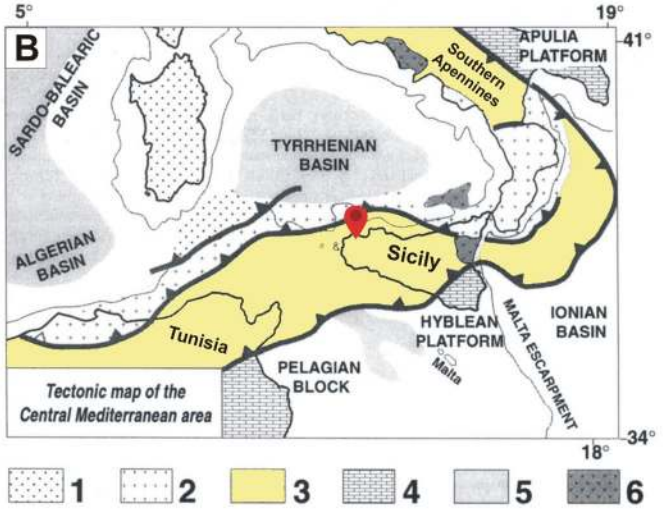
B
5°
19°
41°
34°
18°
SARDO-BALEARIC BASIN
APULIA PLATFORM
Southern Apennines
TYRRHENIAN BASIN
ALGERIAN BASIN
Sicily
Tunisia
HYBLEAN PLATFORM
MALTA ESCARPMENT
IONIAN BASIN
PELAGIAN BLOCK
Malta
Tectonic map of the Central Mediterranean area
1
2
3
4
5
6

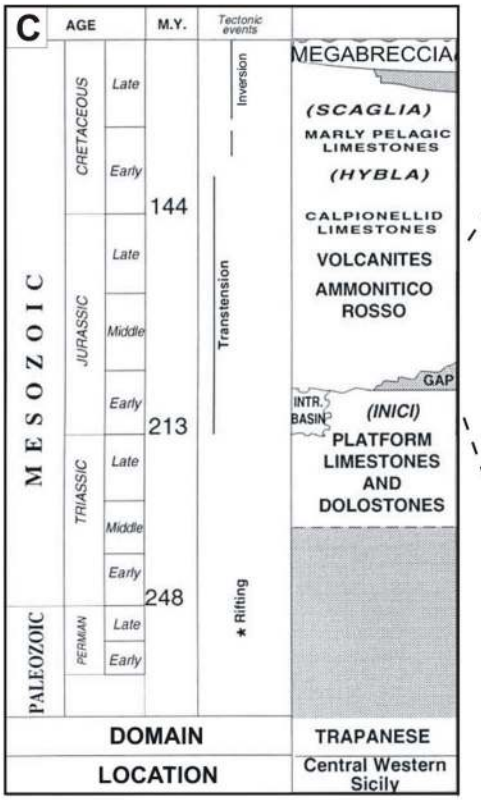
C
AGE
M.Y.
Tectonic events
MESOZOIC
PALEOZOIC
CRETACEOUS
JURASSIC
TRIASSIC
PERMIAN
Late
Early
Middle
144
213
248
Inversion
Transtension
Rifting
MEGABRECCIA
(SCAGLIA)
MARLY PELAGIC LIMESTONES
(HYBLA)
CALPIONELLID LIMESTONES
VOLCANITES
AMMONITICO ROSSO
GAP
INTR. BASIN
(INICI)
PLATFORM LIMESTONES AND DOLOSTONES
DOMAIN
TRAPANESE
LOCATION
Central Western Sicily

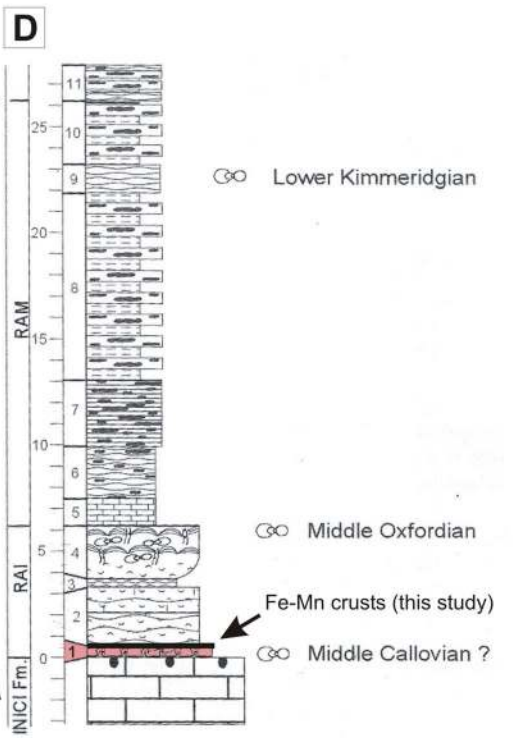
D
RAM
RAI
INICI Fm.
Lower Kimmeridgian
Middle Oxfordian
Fe-Mn crusts (this study)
Middle Callovian ?


E
2.5m

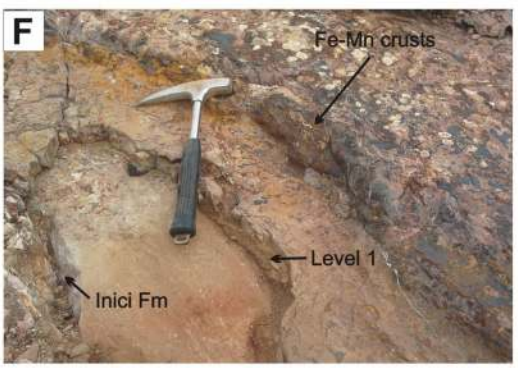
F
Fe-Mn crusts
Level 1
Inici Fm

◂**Fig. 1** **a** Location (in red) of the studied Fornazzo section (Monte Inici); **b** Tectonic map of the central Mediterranean (modif. from Catalano et al., 1996): (1) Corsica-Sardinia; (2) Calabro-Kabilian Arc; (3) Marghrebian-Sicilian-Southern Apennine nappes and deformed foreland; (4) foreland and mildly folded foreland; (5) areas with superimposed extension; (6) Plio-Quaternary volcanism; **c** Chronostratigraphy of the Trapanese succession (modif. from Catalano et al. 1996; time scale according to Harland et al. 1990); **d** Lithostratigraphy of the Fornazzo quarry (modif. from Martire and Pavia 2002); in pink the condensed "level 1" (see text) and in black the Fe–Mn encrusted bed object of this study (arrow); **e** View of the disused Fornazzo quarry with the Fe–Mn encrusted bed at the floor; **f** Close-up view of the quarry floor with detail of the stratigraphic position of the Fe–Mn crusts with respect to the Inici Fm and the "level 1"

(see next section). Thin sections were obtained by standard methods and observed under a Leica polarized-light microscope. Scanning Electron Microscope (SEM) investigations were performed on carbon-coated samples, using a LEO 440 with EDS (Energy Dispersive Spectroscopy) system OXFORD ISIS 300 Link and Si (Li) PENTAFET detector. Bulk mineralogy was determined by powder X-ray diffraction (XRD) using a Philips PW14 1373 with a Cu-Kα radiation filtered by a monochromator crystal and a 2° 2θ/minute scanning speed. Stable C and O isotope composition was determined on powders collected using a micro drill, from the different sample portions. CO_2 was obtained by classical H_3PO_4–$CaCO_3$ reaction method, at 50 °C, by an automated Carbonate Preparation Device (Thermo Scientific GasBench II). Isotopic ratios were measured by Thermo Scientific Delta V Advantage continuous flow mass spectrometer. Results are reported with typical delta (δ) notation relative to the V-PDB standard. The relative precision for duplicate analyses improved to 0.1‰ for carbon and oxygen.

Geochemical elemental analyses were performed at ActLabs Ltd (Ancaster, ON, Canada). The determination of major and minor elements (oxide) was carried out by RX Fluorescence (XRF). To minimize the matrix effects of the samples, the heavy absorber fusion technique (Norrish and Hutton 1969) was used. Prior to fusion, the loss on ignition (LOI), which includes H_2O^+, CO_2, S and other volatiles, was determined from the weight loss after roasting the sample at 1000 °C for 2 h. The fusion disk was made by mixing a 0.75 g equivalent of the roasted sample with 9.75 g of a combination of lithium metaborate and lithium tetraborate, with lithium bromide as a releasing agent. Samples were fused in Pt crucibles using an automated crucible fluxer and automatically poured into Pt molds for casting and analyzed on a Panalytical Axios Advanced wavelength dispersive XRF. Detection limit was 0.01 wt% for all the elements. On three samples, selected as representative of the main lithologies identified on the base of macroscopic and mineralogical features, Rare Earth Elements and Y (REY) were determined by Perkin Elmer Sciex ELAN 6000, 6100 and 9000 ICP/MS. In consideration of the nature of samples, characterized by stronghly refractory minerals, an aggressive technique employing a lithium metaborate/tetraborate fusion was applied. Samples were mixed with a flux of lithium metaborate and lithium tetraborate and fused in an induction furnace. The obtained melt was immediately poured into a solution of 5% nitric acid containing an internal standard, and mixed continuously until it completely dissolved (~45 min). The samples were run by a combination simultaneous/sequential Thermo Jarrell-Ash ENVIRO II ICP or a Varian Vista 735 ICP. Calibration is performed using 14 prepared USGS and CANMET certified reference materials. One of the 14 standards is used during the analysis for every group of ten samples. Detection limit was 0.01 mg/kg for Lu, 0.05 mg/kg for Pr, Eu, Tm, 0.1 mg/kg per La, Ce Nd, Sm, Gd, Tb, Dy, Ho, Er, Yb and 1 mg/kg for Y.

Results

Macroscopic features and mineralogy

Fe–Mn concretions from the Fornazzo section form mostly continuous millimeter to centimeter-thick pavement just at the top of the Rosso Ammonitico basal condensed level (Fig. 1d, f). It is characterized by frequently mammilated surface, expression of an internal architecture constituted by laminated columns or pseudocolumns, several millimeters wide, consisting of stacked hemispheroids. Field observations give evidence of a basic morphology recognizable to the naked eye and represented by flat to ondulose stromatolitic crusts of variable thickness (Fig. 2a).

Sectioned and hand polished specimens were selected, divided in sub-samples and grouped in three different lithologies on the base of macroscopic texture, color and mineralogy (Table 1; Figs. 2 and 3):

- Limestone, represented by sample HI 1a, consists of consolidated calcilutite showing an homogeneous pink color; it is almost completely constituted by calcite (97.8%) with trace of quartz (< 1%) and hematite (1.4%), the latter identified at 2.69 Å (104 reflection). This sample is considered in the discussion as the geochemical background to evaluate variations and enrichments in trace elements and REY;
- Dendrites in limestones (samples HI 1b, 2a, 2b, 3a, 3b and 4a) are characterized by the presence of dark micro-dendrites arranged in sub-layers less than 5 mm in thickness, in columnar growth patterns or in dome structure. Due to the presence of micro-dendrites, the powered samples are characterized by an almost grayish color (Table 1). All samples are constituted by predominant calcite (91.8% in average), moderate quantity of hematite

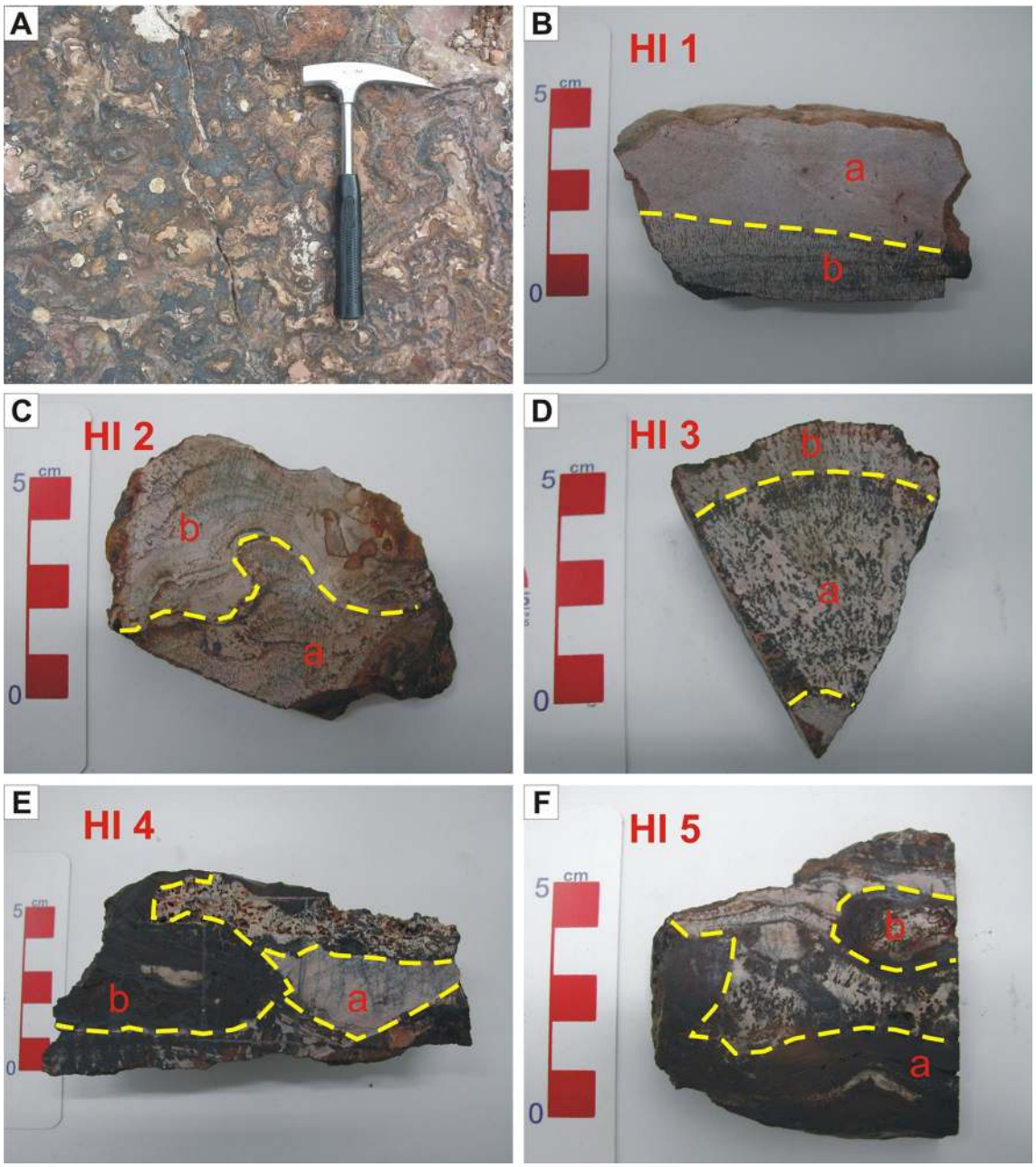

Fig. 2 **a** Close-up view of the Fe–Mn encrusted bed at the floor of the quarry; **b–f** Samples object of this study. Dotted lines delimite sub-samples: limestone (1a), dendrites in limestone (1b, 2a, 2b, 3a, 3b, 4a) and Fe–Mn crusts (4b, 5a, 5b)

with an average value of 2.8% and by pyrolusite, detected at 3.14 Å (110 reflection), in particular in sample HI 1a and 3a (4.8 and 3.5%, respectively). Other mineralogical phases, present in trace, are todorokite with the main peak at 9.65 Å (100 reflection), birnessite identified by a peak at 7.09 Å (002 reflection), carbonate-fluorapatite (main reflection at 2.79 Å) and quartz;

- Fe–Mn crusts, grouping samples HI 4b, 5a and 5b, are characterized by a dark color and parallel dense lamination consisting of millimetric dark brown to black layers with a slightly different metallic to submetallic lustre surface. These samples are mineralogically characterized by high content of hematite (43.5% in average), up to 51.3% in sample HI 5a, which also shows the highest percentage of quartz (2.9%). In this sample, the presence of todorokite and pyrolusite is not detected, which, on the contrary, were both recognized in samples HI 4b and 5b with the predominance of todorokite (values of 4.8 and 5.2%, respectively). All

Table 1 Samples object of this study with indication of the color from the Munsell Soil Color Charts and the used method for the chemical analyses

Lithology	Sample	Munsell color	Chemical analyses method
Limestone	HI 1a	5YR 8/2	Fusion-ICP
Dendrites in limestone	HI 1b	10YR 4/1	Fusion-ICP
	HI 2a	5YR 4/2	Fusion-XRF
	HI 2b	5YR 4/3	Fusion-XRF
	HI 3a	10YR 3/2	Fusion-XRF
	HI 3b	10YR 3/1	Fusion-XRF
	HI 4a	10YR 4/1	Fusion-XRF
Fe-Mn crusts	HI 4b	2.5YR 1.7/1	Fusion-XRF
	HI 5a	2.5YR 2/1	Fusion-ICP
	HI 5b	7.5YR 3/2	Fusion-XRF

these samples contain birnessite, especially samples HI 5a and 5b (percentage of 4.4 and 3.7%, respectively).

Petrography

Textural features, defined by observations of samples under the petrographic microscope with reflected light and by the SEM, were described with respect to the three different lithologies identified on the base of macroscopic features and mineralogical composition.

Limestone

Sample HI 1a can be classified as packstone/wackstone (Fig. 4a; Dunham 1962) on the base of the relationship between bioclasts and mud, evaluable under the polarized light microscope. This sample is referable to the lowest condensed Rosso Ammonitico level, biostratigraphically described in detail by Wendt (1963) and Martire and Pavia (2002). As a whole, bioclasts are represented by fragments of ammonites, lamellibranchs, belemnites, crinoids, and foraminifera and observation with reflected light shows that bioclasts, in particular foraminifera and ammonoid, often appear, completely or partially, filled by hematite which is also recognizable as sub-micrometric crystals dispersed in the micritic matrix (Fig. 4b). The dispersion of the hematite in the matrix causes the pigmentation, grading from pink to deep red.

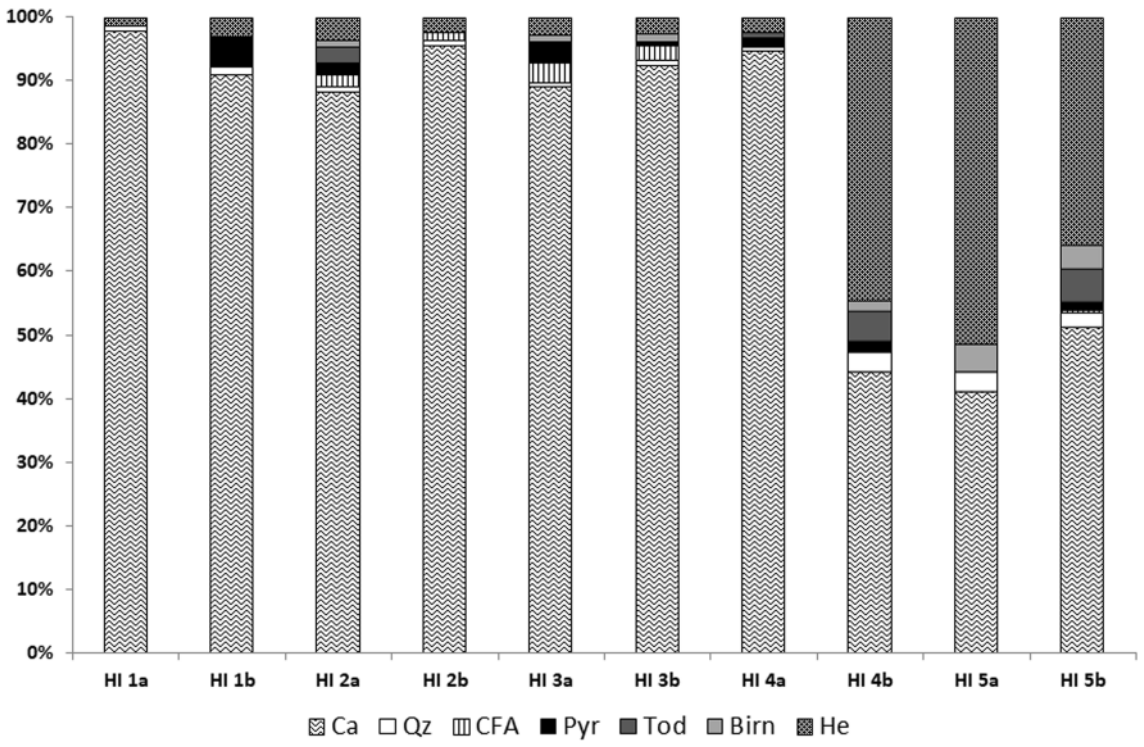

Fig. 3 Mineralogical composition of the Fornazzo samples. Ca: calcite; Qu: quartz; CFA: carbonato-fluorapatite; Pyr: pyrolusite; Tod: todorokite; Birn: birnessite; He: hematite

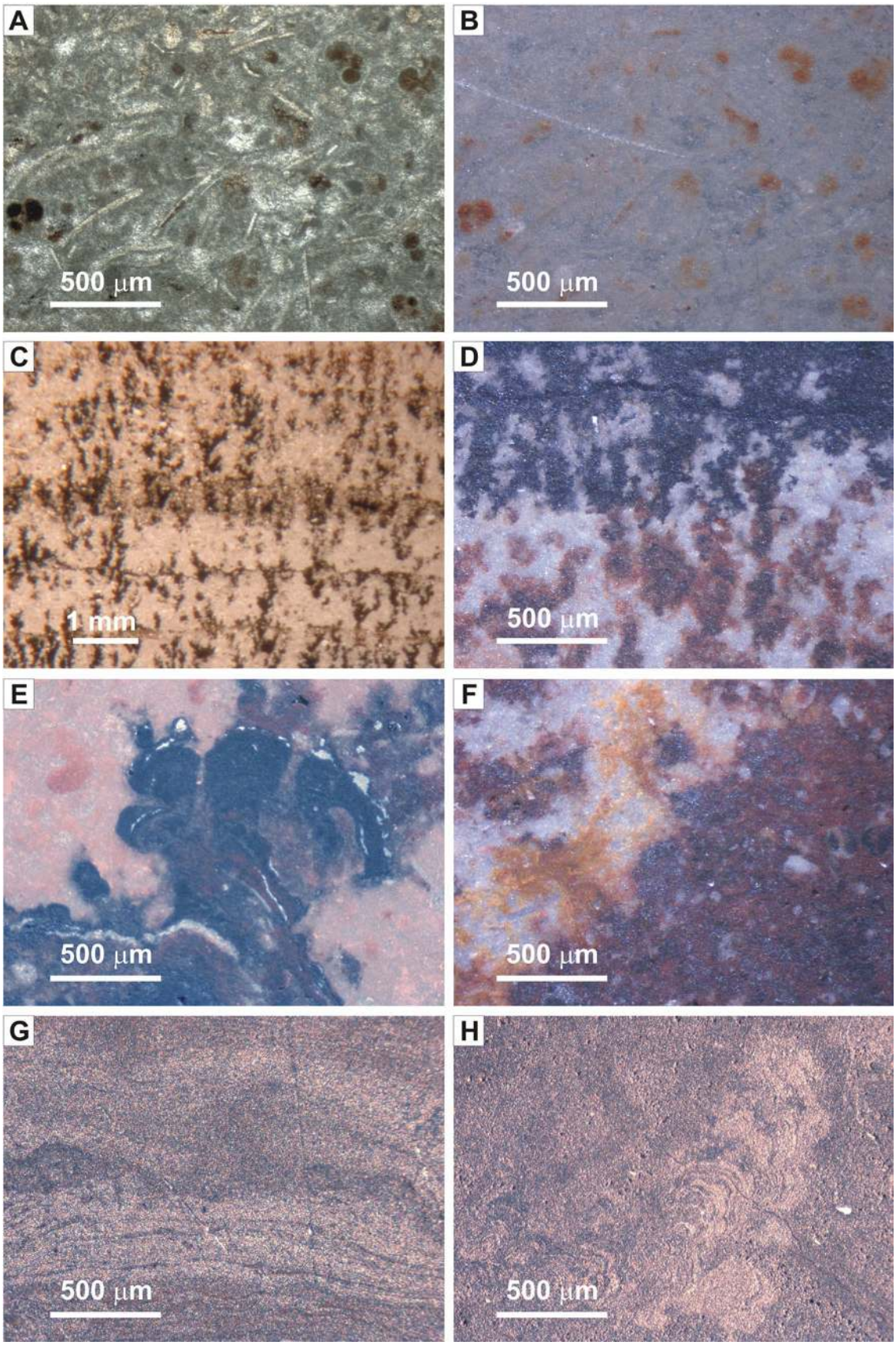
A
500 μm
B
500 μm
C
1 mm
D
500 μm
E
500 μm
F
500 μm
G
500 μm
H
500 μm

◂**Fig. 4** **a**–**b** Micrographs of the Rosso Ammonitico limestone (sample HI 1a) showing bioclasts filled by hematite; **c, d** Dark dendrites growing up orthogonally to the lamination and detail of branches passing from reddish brown to black color (sample HI 1b); **e** Digitate texture produced by the overlapping of "half-moon" constructions (sample HI 3a); **f** Yellow/orange coating; **g, h** Dense horizontal and subparallel lamination with local knobby/digitate arrangement in a Fe–Mn crust (sample HI 5a). **a** Plane polarized light, **c** Stereo microscope, **b**, **d**–**h** Reflected light

Dendrites in limestones

Presence of dark dendrites growing up orthogonally to the lamination is the main feature of this group of samples (Figs. 3 and 4c). Particularly regular arborescent structures are documented in sample HI 1b, which, in reflected light, appear constituted by branches passing from reddish brown to black color (Fig. 4d), expression of a different mineralogical composition (hematite and pyrolusite, respectively). Besides the arborescent structures, sample HI 3a also shows micro-columnar/digitate structures produced by the overlapping of "half-moon" constructions (Fig. 4e) with variable mineralogical composition. In some portions, yellow/orange coating are probably referred to iron hydroxides, later recrystallized in hematite (Fig. 4f).

Observation under the SEM confirms the presence of dome and stromatolitic texture, where overlapped laminae are characterized by an alternation between compacted and more porous layers (Fig. 5a). Both of them appear fairly recrystallized and microstructures, of potential microbial origin, are not recognized. As for the composition, observation by backscattered electrons detector (QBSD) and EDS analyses documents the predominance of manganese in light grey layers (Fig. 5b) consisting of acicular crystals, likely of todorokite (Fig. 5c). More porous lamina, grey at QBSD, show a higher content in iron, while the lightest lamina are characterized, in the EDS spectrum, by a moderate peak of barium, probably referable to the romanechite [$(Ba, H_2O)_2(Mn^{4+}, Mn^{3+})_5O_{10}$] (Fig. 5b, d). Finally, in limited portion of same sample, microspheroid of carbonate-fluorapatite are identified in association with calcite (Figs. 5e, f).

Fe–Mn crusts

Fe–Mn crusts are mainly constituted by dark dense horizontal and subparallel lamination (Fig. 4g), which locally may occur as columnar/digitate arrangement. In particular, flat lamination seems to pass gradually to slightly undulate crusts, then changing outward to pseudo-columnar or digitate morphologies (Fig. 4h).

Lamination in sample HI 5a is well evident under the SEM at QBSD (Fig. 6a, b). Alternation of dark and light laminae relates to different content in Mn, Fe and Ba but a predominance of iron is documented (Fig. 6c). Particularly interesting is a very light lamina whose EDS spectrum highlights the presence of Ce associated with Fe (Fig. 6b, d). As for the textural features observable at secondary electrons (SE), peculiar micro-textures are documented in sample HI 4b. Figure 6e, f shows a nubby matrix in which straight to slightly curved filaments, about 1 µm in diameter and more than 0.5 mm in length, are evident. In other portions, aggregates of coccoid-shaped particles, with a maximum size of ~1 µm, gradually pass to acicular microcrystals attributable to todorokite (Fig. 6g, h).

Geochemistry

Major and trace elements

Concentrations of major and selected trace elements determined in the Fornazzo samples are listed in Table 2. All the elements, except Ca and P, show a general increase in concentration from limestone to dendrites and further to crusts (Fig. 7).

In particular, in the limestone (sample HI 1a), besides the Ca with concentration of 38.48%, all major elements are present in concentration less than 1%; similarly, trace elements are nearly absent with the exception of Ni reaching the value of 50 mg/kg.

In the dendrites, a light decrease in Ca, passing at an average value of 34.22%, is documented; among other major elements, Fe and, to a greater extent, Mn show an increase, the latter up to 12.32% in sample HI 3a. In the same sample, the uppermost trace elements concentrations with respect to this typology of samples are also recorded. Moreover, samples HI 3a and 3b document the highest content in P (0.31 and 0.27%, respectively), reflecting the presence of carbonato-fluorapatite, recognized by XRD analyses and detected by SEM observation (Figs. 3, 5e, f).

Finally, in the Fe–Mn crusts, the average value of Ca drops to 17.80%, while all other elements exhibit sharp increase, in particular Fe and Mn for the major elements (average values of 10.66 and 16.93%, respectively) and Ni, V and Zn for the trace elements.

To better define the factors controlling the element geochemical behavior and the relationship with the recognized mineralogical phases, a multivariate statistical analysis was applied at the bulk geochemical dataset. Cluster analisys (CA), processed with respect to elements (Fig. 8), highlights two main groups separating Cu, P, Ca (cluster 1) from all others elements (cluster 2). Cluster 2 is then significantly subdivided in two sub-clusters: 2A and 2B which discriminate V, Ti, Fe from Zn, Co, Mn and further from Ni, Al, K, Mg and Si.

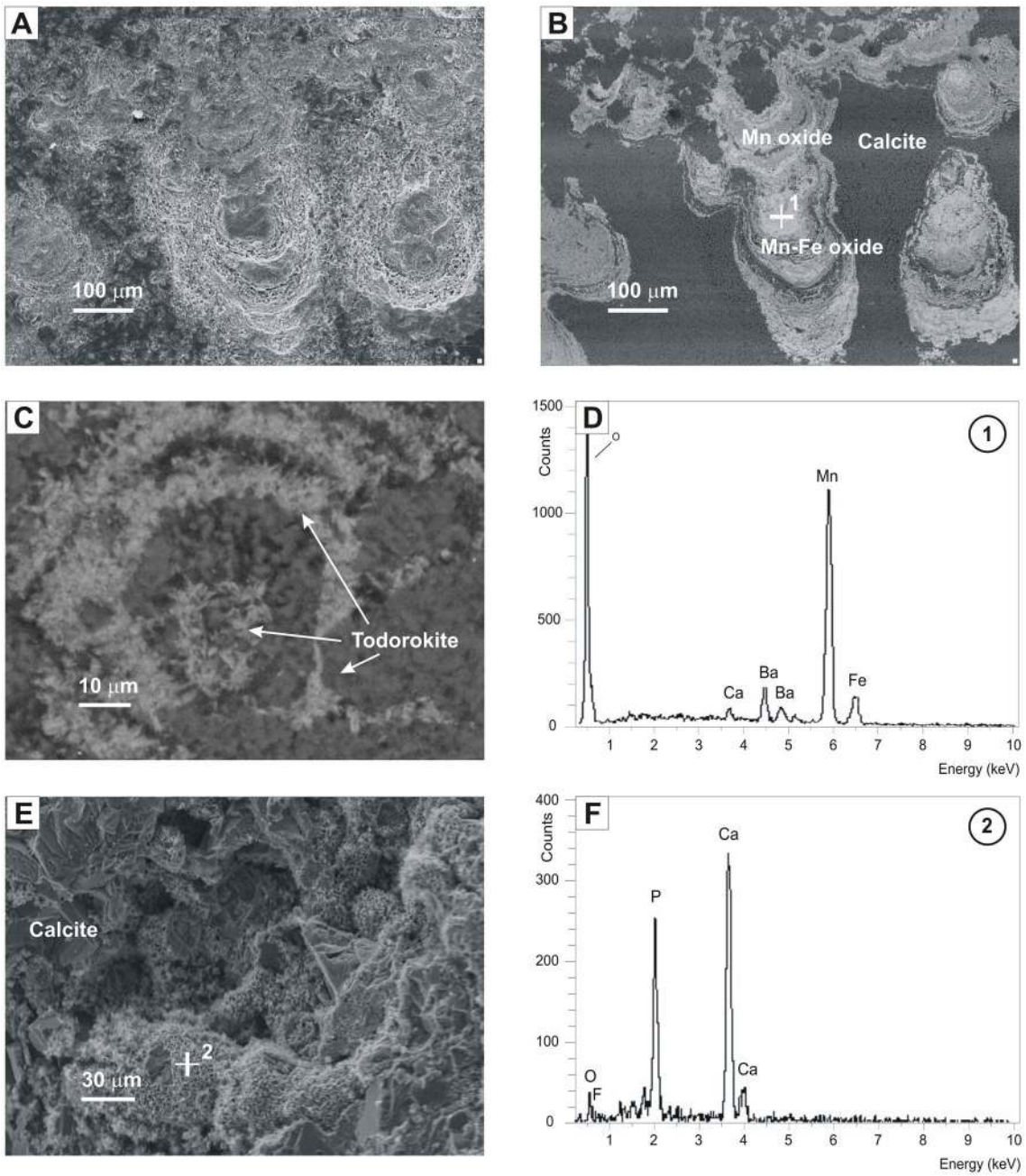

Fig. 5 SEM images and EDS spectra of the dendrites samples: **a**, **b** Overlapped laminae forming dome and stromatolitic texture of different chemical composition; EDS spectrum of spot 1 is shown in (**d**); **c** Light grey acicular crystals of todorokite; **e** microspheroids of carbonate-fluorapatite (spot 2) identified by EDS spectrum in **f**. **a** and **e** SE detector, **b** and **c**: QBSD detector

REE and Y

In the study of marine Fe–Mn crust and nodules, the rare earths and yttrium (REY) have been extensively used to discriminate the genetic conditions and the rate of crust growth (Jach and Dudek 2005; Hein et al. 2008; Reolid 2011; Loges et al. 2012; Bau et al. 2014; Wang et al. 2015; Marino et al. 2017). Among this wide literature, Bau et al. (2014) propose easy-to-use, robust discrimination diagrams based on geochemical relationships controlling the REY inventory of marine Fe–Mn oxy-hydroxides deposits. Moreover, according to Bau (1996), due to similarity of ionic radius to Ho^{3+} and Y^{3+}, it was chosen to insert Y into REE patterns between isovalent Dy^{3+} and Ho^{3+}. For this study three samples, one for each typology (limestone, dendrites and Fe–Mn crusts), were selected to carry out the REY determination. First of

all, also to evaluate the quality of the analysis, obtained concentrations was normalized with respect to the shale (the Post-Archean Australian Shale, PAAS, of McLennan 1989). Actually, normalization removes the pronounced 'zig-zag' pattern caused by the differences in abundance between even and odd atomic numbers; therefore, a deviation from the expected smoothness of shale normalized (SN) REY pattern (REY_{SN}) could be related to an analytical error. The only exception to this rule is represented by redox-sensitive Ce and Y because of subtle differences among the stabilities of chemical REY complexes. The REY_{SN} pattern for the selected Fornazzo samples (Fig. 9a) shows that: (i) except for anomalies of Ce and Y, explained by the physico-chemical properties of the respective elements (see discussion), all the REY_{SN} patterns are smooth, indicating excellent analytical quality, and (ii) REY_{SN} concentration are higher in Fe–Mn crust with respect to limestone and dendrites. Finally, following Bau et al. (2014), three robust proxies, proposed to discriminate the genetic types of marine Fe–Mn deposits, were considered (Figs. 9b, c): Nd concentrations, Y_{SN}/Ho_{SN} ratio and Ce_{SN}/Ce_{SN}* ratio, where $Ce_{SN}^* = 0.5La_{SN} + 0.5Pr_{SN}$.

Stable isotope geochemistry

The values of carbon and oxygen stable isotopes for the Fornazzo samples are listed in Table 2 and shown in Fig. 10. The values obtained are in the range of – 1.42 and – 0.38‰ for $\delta^{18}O$ and between 1.06 and 2.71‰ for $\delta^{13}C$. Only one sample (HI 4b) shows slight lower values of the oxygen and carbon isotope ratio (− 2.40 and − 0.25‰, respectively).

Discussion

Genetic origin

The Jurassic Fe–Mn concretions, mostly formed on seamounts or other isolated places, are generally related to sea-level rise or sea-level highstand. They result from considerable drop of terrigenous influx and reduced sedimentation, and frequently show association with bacterial stromatolites and sessile foraminifers (Jenkyns 1970b; Ballarini et al. 1994; Dromart et al. 1994; Jiang et al. 2019). Such occurrences are commonly associated to condensed sediments, which, in the Fornazzo section, are represented by the Rosso Ammonitico facies. There is little doubt about the submarine origin of the Fe–Mn crusts but, to rule out any doubts about the relationship with subaerial origin or a late meteoric diagenesis, carbonate stable isotope composition of the Fornazzo samples was considered. Figure 10 shows that all samples safely plot within the general field of the Jurassic marine carbonates (as measured by Veizer et al. 1999). Only one point (sample HI 4b) is characterized by a lighter composition in oxygen and carbon isotopes, but, however, in the range of marine carbonate. This is probably due to a mixture of isotopically heavier primary marine carbonate with isotopically lighter early diagenetic cement. The lower $\delta^{13}C$ is compatible with the introduction of ^{12}C from the organic matter oxidation, while lower $\delta^{18}O$ ratio may be interpreted as the result of recrystallization at slightly higher temperature associated with burial.

Regarding the origin of the Fe–Mn crusts, it may be considered under three main processes: hydrogenetic, diagenetic, and hydrothermal (Glasby 2000; Jach and Dudek 2005; Rajabzadeh et al. 2017). Hydrogenetic deposits form directly from seawater in oxidizing environment and are characterized by slow growth between 1 and 15 mm/Myr. Diagenetic deposits result from early-diagenetic processes involving metals supplied from underlying sediments and precipitate close to the sediment/water interface. They are generally characterized by faster growth rates of 10's to 100's mm/Myr. Hydrothermal deposits precipitate directly from hydrothermal solutions in areas with heat flow and are characterized by high to extremely high growth rates also above 1000 mm/Myr (cf. Segl et al. 1984; Manheim 1986; Puteanus and Halbach 1988).

Discrimination of the main process responsible for the Fe–Mn oxy-hydroxides precipitation is mostly carried out on geochemical base, beginning from the distribution of Fe and Mn. In the Fornazzo samples, although both of elements seem strongly enriched in Fe–Mn crusts, this increase is most likely magnified by the carbonate dilution effect (Fig. 7). To remove this influence, the Mn/Fe ratio has been considered, showing an averagely higher value in the dendrites coupled with higher content of pyrolusite (Figs. 3 and 7). Mn-oxides are generally associated to biogeochemically mediated epigenetic events, by which primary Mn deposits underwent remobilization/redeposition processes (Rajabzadeh et al. 2017). The presence of carbonate-fluorapatite in this typology of samples testifies phosphogenesis processes typical of early diagenesis and considered from many authors induced by bacterial mediation (Lucas and Prévôt 1985; Froelich et al. 1988; Lamboy 1990; Sanchéz-Navas and Martín-Algarra 2001; Scopelliti et al. 2010). Conversely, Mn-oxy-hydroxides (todorokite and birnessite), together with high percentage of hematite, the latter probably derived by recrystallization of goethite, prevail in Fe–Mn crusts, where the Mn/Fe ratio decrease (Figs. 3 and 7). These mineral phases are commonly related to oxy-hydroxides colloids involved in the first stage of hydrogenetic precipitation (Marino et al. 2019). Finally, sulfides, authigenic mixed-layer clays, or opaline silica, generally associated to hydrothermal deposits (e.g.,Jach and Dudek 2005; Marino et al. 2018), are not documented in the Fornazzo samples.

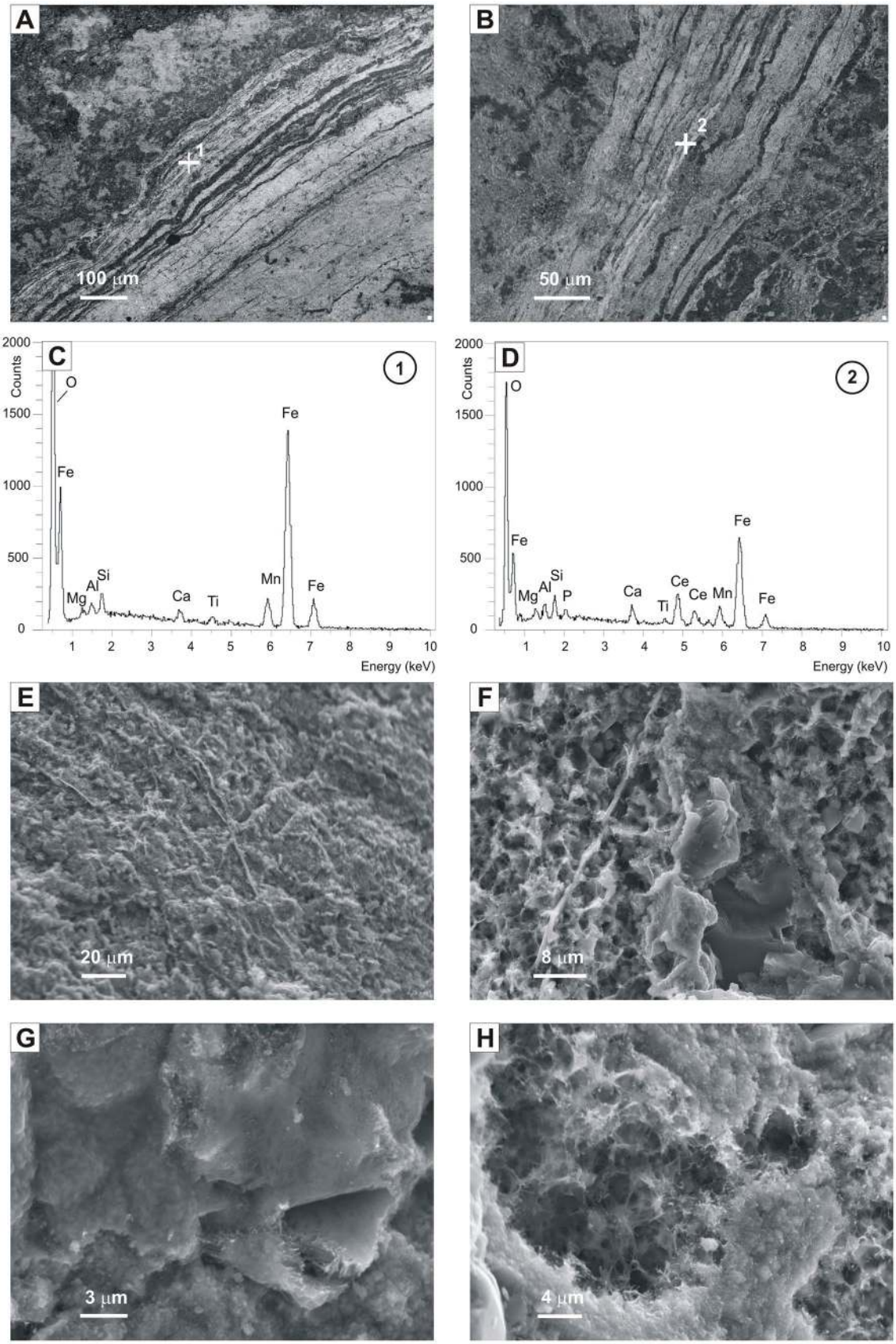
A
1
100 μm
B
2
50 μm
C
1
Counts
2000
1500
1000
500
0
O
Fe
Mg
Al
Si
Ca
Ti
Mn
Fe
Fe
1 2 3 4 5 6 7 8 9 10
Energy (keV)
D
2
Counts
2000
1500
1000
500
0
O
Fe
Mg
Al
Si
P
Ca
Ti
Ce
Ce
Mn
Fe
Fe
1 2 3 4 5 6 7 8 9 10
Energy (keV)
E
20 μm
F
8 μm
G
3 μm
H
4 μm

◂**Fig. 6** SEM images and EDS spectra of the Fe–Mn crusts: **a**, **b** Alternation of dark and light laminae prevalently constituted by Fe (spot 1); **c**, **d** EDS spectra of spot 1 and 2, in the latter is evidenced the presence of Ce; **e**, **f** straight to slightly curved filaments in a nubby matrix; **g**, **h** aggregates of coccoid-shaped particles gradually passing to acicular microcrystals of todorokite. **a** and **b**: QBSD detector; **e**–**h**: SE detector

According to a detailed study of Marino et al. (2018), the multivariate analysis performed on major and trace elements reveals the presence of two main groups clearly linked to the main mineralogical phases (Fig. 8). Elements of cluster 1 are strictly associated with phosphates and carbonate biogenic particles and elements grouping in cluster 2 are related to Fe–Mn oxy-hydroxides. More in detail, subcluster 2a, grouping Fe with V and Ti, represents the Fe oxy-hydroxides colloids involved in the hydrogenetic precipitation. The slightly positive charge of the iron hydroxide surface is thought suitable to bind the vanadium (Koschinsky and Halbach 1995; Hein et al. 1997), while following Koschinsky and Halbach (1995), titanium probably inter-grew as $TiO_2{\cdot}2H_2O$ together with the amorphous FeOOH phase. Conversely, subcluster 2b discriminate the elements bonded to the Mn-oxides/oxy-hydroxides and, subordinately, related to the clay fractions or substrate rock. In this way, the association of Mn with Co, Zn and Ni ($r = 0.95$, 0.92 and 0.90, respectively) is usually attributable to hydrogenetic origin and/or to biomineralization processes (Abad et al. 2010; Marino et al. 2017; Jiang et al. 2019); the greater linkage distance of Ni from Mn is probably related to the release of nickel to the porewaters during the early diagenesic transformation of birnessite to todorokite (Atkins et al. 2016).

As for the trace elements, a widely used method to distinguish the genetic origin of Fe–Mn deposits is the Fe–Mn–(Ni + Co + Cu)*10 ternary diagram (Bonatti et al. 1972), in which the hydrothermal deposits plot close to the base line, while higher Ni, Co and Cu contents are indicative of an increasing hydrogenetic influence. Consistently with the above considerations, Toth (1980) modified the ternary diagram of Bonatti et al. (1972) adding the diagenetic field near the manganese apex. In the studied samples, two of three Fe–Mn crusts distinctly plot in the hydrogenetic field, while others fall between hydrogenetic and diagenetic fields (Fig. 11). None of them presents concentrations in the range of those characteristic of hydrothermal origin (Glasby 2000).

To better discriminate and characterize the three typologies of the Fornazzo Fe–Mn concretions, PAAS normalized REY pattern and discrimination diagrams proposed by Bau et al. (2014) are shown in Fig. 9. Uniquely among the REE, Ce may form a tetravalent ion under appropriate oxidizing conditions. The oxidized form of Ce (Ce^{4+}) is relatively insoluble compared to Ce^{3+} (e.g.,de Baar et al. 1985; Hein et al. 2000; Astakhova and Sattarova 2012), so that Ce takes part in active redox cycling. During the hydrogenetic precipitation, the Ce uptake by colloidal Mn and Fe oxy-hydroxides is accompanied by the Ce oxidation, which is mediated by surface catalysis. The oxidative scavenging of Ce results in the development of a positive Ce anomaly. In this study, the same pattern is characteristic of sample HI 5a, representing the Fe–Mn crusts (Fig. 9a).

Since Ce is preferentially scavenged by oxy-hydroxides, the Ce content in ocean seawater is generally low with a distinct negative anomaly (Bogdanov et al. 1995; Ren et al. 2011; typical deep seawater from Bao et al. 2008 is reported in Fig. 9a), this anomaly is inherited by the rapid scavenge of REY from the seawater when the Fe–Mn hardground precipitate very close to the hydrothermal vent sites. In this case, the only preserved hydrothermal signature is the positive Eu_{SN} anomaly due to a process of leaching of Eu^{2+} from the host rocks at temperatures above 250 °C (German et al. 1990, 2002; Mitra et al. 1994; Bau and Dulski 1999; Sherrell et al. 1999; Edmonds and German 2004; Marino et al. 2018). None of the studied samples shows positive Eu anomaly while the negative Ce anomaly, reflecting seawater inherited REY patterns, is documented in limestone (sample HI 1a).

The REY_{SN} pattern of diagenetic Fe–Mn crusts allows to discriminate this type of Fe–Mn deposits from those of hydrogenetic origin, because in marked contrast to the latter, they record a negative Ce anomalies and lower REY concentrations (Bau et al. 2014). These features are matched in sample HI 1b, which represents dendrites in limestone (Fig. 9a). As suggested by Bau et al. (2014), Mn forming dendrites should result from the mobilization and re-oxidation of tri- and tetravalent Mn of marine sediment, first reduced and dissolved during early diagenesis processes. The negative Ce anomaly of diagenetic deposits should, therefore, indicated that while sub-oxic porewaters mobilized Mn^{2+} and REY^{3+}, Ce^{4+} remained fixed in discrete Ce(IV) compounds. Fluctuating redox conditions should also be responsible of phosphogenetic processes, because it is documented that the oxy-hydroxides redox cycle promotes phosphate sink-switching mechanism (Froelich et al. 1988; Jarvis et al. 1994; Piper and Perkins 2004; Scopelliti et al. 2010).

Having ruled out the hydrothermal origin for Mn-dendrites and Mn-Fe crusts and verified the coherence of Fornazzo limestone REY pattern with the seawater signal, to further discriminate diagenetic from hydrogenetic origin of the two typologies of the studied samples, Y anomaly, Y_{SN}/Ho_{SN} ratio, Ce_{SN}/Ce_{SN}* ratio and Nb concentration are now considered (Fig. 9b, c). Actually, the hydrogenetic origin of sample HI 5a is highlighted, in addition to the positive anomaly of redox-sensitive Ce, also by the well-marked Y negative anomaly, due to the decoupling of the geochemical twins Y and Ho. This decoupling results from preferential scavenging of Ho relative to Y on oxy-hydroxides surfaces, due to lower stabilities of Y surface complexes (e.g., Bau

Table 2 Chemical and stable isotope compositions of the Fornazzo samples

		HI 1a	HI 1b	HI 2a	HI 2b	HI 3a	HI 3b	HI 4a	HI 4b	HI 5a	HI 5b
Si	(wt %)	0.13	0.27	0.39	0.22	0.38	0.31	0.22	1.31	1.11	0.56
Al	(wt %)	0.10	0.25	0.55	0.40	0.60	0.48	0.37	1.67	1.12	0.77
K	(wt %)	0.02	0.02	0.00	0.00	0.02	0.00	0.01	0.17	0.14	0.06
Ti	(wt %)	0.01	0.01	0.02	0.02	0.01	0.01	0.04	0.12	0.31	0.10
Mg	(wt %)	0.27	0.45	0.35	0.43	0.52	0.46	0.29	1.42	1.17	0.76
Ca	(wt %)	38.48	35.99	34.89	35.94	28.11	35.31	35.12	16.49	13.34	23.56
P	(wt %)	0.04	0.05	0.17	0.10	0.31	0.27	0.05	0.04	0.10	0.20
Fe	(wt %)	0.19	0.41	2.18	0.82	2.01	1.16	1.22	6.18	19.56	6.25
Mn	(wt %)	0.12	3.34	2.87	2.65	12.32	3.88	4.53	20.72	15.59	14.48
Co	(mg/kg)	11.0	213.0	161.5	220.3	1138.0	469.9	279.0	2518.3	2734.0	1718.0
Cu	(mg/kg)	0.0	90.0	103.8	21.0	191.7	143.8	47.9	303.5	60.0	47.9
Ni	(mg/kg)	40.0	850.0	573.6	667.9	1885.9	982.3	392.9	10561.2	5610.0	3363.2
V	(mg/kg)	12.0	33.0	78.4	39.2	196.1	72.8	151.3	560.2	1318.0	493.0
Zn	(mg/kg)	3.0	60.0	11.6	61.0	265.3	142.4	116.3	765.8	780.0	853.0
La	(mg/kg)	16.3	19.8	–	–	–	–	–	–	269.0	–
Ce	(mg/kg)	7.1	26.4	–	–	–	–	–	–	2260.0	–
Pr	(mg/kg)	2.8	3.1	–	–	–	–	–	–	45.3	–
Nd	(mg/kg)	11.3	12.1	–	–	–	–	–	–	170.0	–
Sm	(mg/kg)	2.1	2.4	–	–	–	–	–	–	35.0	–
Eu	(mg/kg)	0.5	0.6	–	–	–	–	–	–	7.7	–
Gd	(mg/kg)	2.0	2.7	–	–	–	–	–	–	30.1	–
Tb	(mg/kg)	0.3	0.4	–	–	–	–	–	–	4.7	–
Dy	(mg/kg)	1.6	2.2	–	–	–	–	–	–	23.8	–
Y	(mg/kg)	12.0	19.0	–	–	–	–	–	–	53.0	–
Ho	(mg/kg)	0.3	0.4	–	–	–	–	–	–	4.0	–
Er	(mg/kg)	0.9	1.2	–	–	–	–	–	–	10.4	–
Tm	(mg/kg)	0.1	0.2	–	–	–	–	–	–	1.4	–
Yb	(mg/kg)	0.6	1.0	–	–	–	–	–	–	8.6	–
Lu	(mg/kg)	0.1	0.1	–	–	–	–	–	–	1.2	–
$Ce_{SN}/Ce_{SN}*$		0.2	0.8	–	–	–	–	–	–	4.7	–
Y_{SN}/Ho_{SN}		1.5	1.7	–	–	–	–	–	–	0.5	–
$\delta^{13}C$	(‰)	2.63	2.68	2.71	2.11	2.28	2.08	2.36	− 0.25	1.57	1.06
$\delta^{18}O$	(‰)	0.03	− 0.54	0.38	− 0.68	− 1.05	− 1.42	0.03	− 2.40	− 0.92	− 0.77

(−): no data

et al. 1995; Bau 1996, 1999; Schijf and Marshall 2011). This anomaly is not shown by the sample representing (diagenetic) dendrites. The decoupling of Ho and Y can be also expressed as Y_{SN}/Ho_{SN} ratio, which can be related to $Ce_{SN}/Ce_{SN}*$ ratio to discriminate hydrogenetic crusts characterized by $Y_{SN}/Ho_{SN} < 1$ from diagenetic deposits displaying negative Ce anomalies ($Ce_{SN}/Ce_{SN}* < 1$), with a negative trend between the two (Fig. 9b). A similar separation is evidenced in a bivariate diagram of the $Ce_{SN}/Ce_{SN}*$ ratio vs Nd concentration (Fig. 9c). Following Bau et al. (2014), diagenetic Fe–Mn deposits show negative to no Ce anomalies and Nd concentrations fall in the range of 10–100 mg/kg, while hydrogenetic Fe–Mn crusts typically show positive Ce anomalies and higher Nd concentrations (> 100 mg/kg).

In summary, geochemical proxies point out for a hydrogenetic origin of Fe–Mn crusts (represented by samples HI 4b, HI 5a and HI 5b and mainly constituted by hematite, todorokite and birnessite), and for a prevalent diagenetic origin of dendrites in limestone (all other samples except sample HI 1a), formed during the early diagenesis, as evidenced by relative increase in Mn (mobilized from the underlying sediments and mainly trapped in form of pyrolusite), and by phosphogenetic processes.

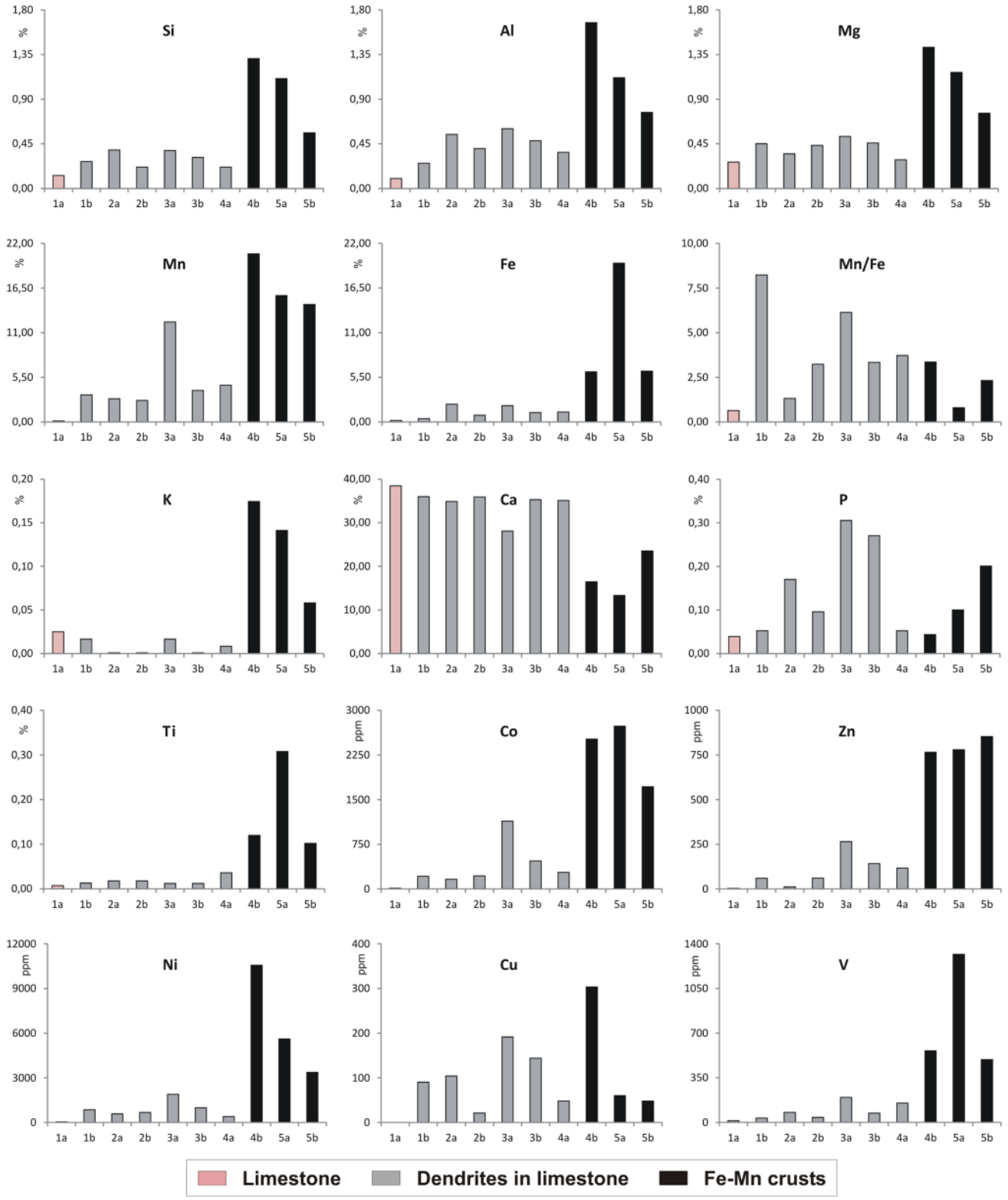

Fig. 7 Distribution of major and trace elements in the Fornazzo samples

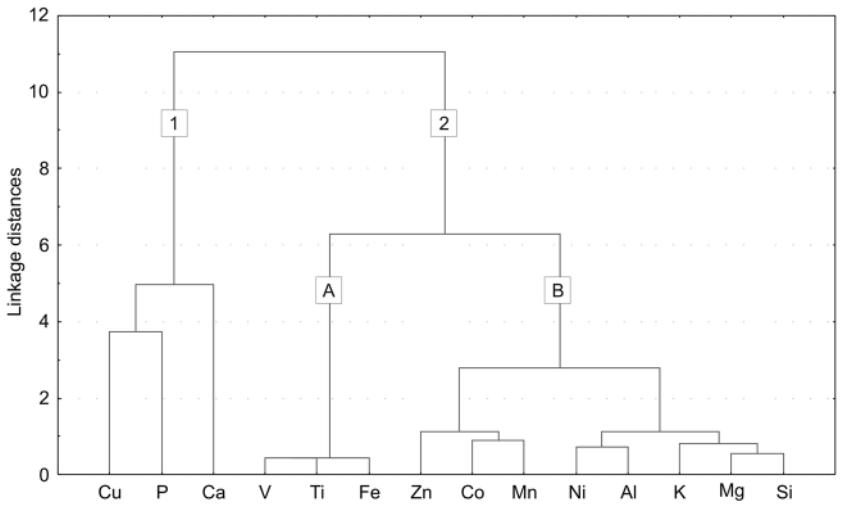

Fig. 8 Cluster analysis performed using the Ward's linkage method based on the Euclidean distances on 14 variables. Numbers and letters identify clusters and sub-clusters (see text)

Growth rates

The REY pattern, discussed in the previous paragraph, is closely connected to the growth rate (GR) of the Fe–Mn deposits that can be discussed both in terms qualitative than quantitative.

First of all, the magnitude of the positive Ce anomaly seems to be strictly related to the crust growth rates because of the slow reaction kinetics of inorganic Ce^{3+} oxidation (Kuhn et al. 1998; Ohta et al. 1999). A slow growth rate is required to produce a positive Ce anomaly (as documented in sample HI 5a), as it has to compensate the negative Ce anomaly of seawater. Moreover, the very slow growth rates of hydrogenetic process allows REY to accumulate in Fe–Mn oxy-hydroxides structures, producing high ∑REY (Bau and Koschinsky 2009). Conversely, a fast growth rate characteristic of Fe–Mn minerals precipitated very close to the hydrothermal vent sites produces a distinct Ce negative anomaly inherited from the seawater pattern. The fast growth rate is also responsible for the extremely low ∑REY (Mills et al. 2001) in this type of deposits.

From the quantitative point of view, to estimate the growth rate (GR) of the Fe–Mn crust and mineralizations from the Fornazzo quarry, is here taken in account the "cobalt chronometer", an algorithm inversely relating the cobalt content and crust GR, widely used for recent Fe–Mn crusts (e.g., Manheim and Lane-Bostwick 1988) but considered accurate also for fossil deposits (Frank et al. 1999). In particular, for crusts with an average Co concentration below about 0.8 wt% (as in the Fornazzo samples), Frank et al. (1999) suggest, as the more appropriate, the equation given by Manheim (1986):

$$GR = 0.68/\left(Co_w\right)^{1.67},$$

where GR is in mm/Myr and Co_w is the Co concentration in wt% less a detrital background concentration of 0.0012 wt%. By applying this equation to the Fornazzo samples, an average growth rate of 8.5 mm/Myr is obtained for the hydrogenous crusts, while an average value of 315 mm/Myr is calculated for the early diagenetic mineralizations. Both of these values are in accord with values defined for these types of Fe–Mn deposits (see previous paragraph).

Microbial contribution

In such a context, the contribution of microorganism activity in the precipitation of Fe–Mn oxy-hydroxides cannot be trascured. The role of microorganism in Fe–Mn nodules and crusts growth was first reported by Thiel (1925). In the following years many studies pointed out for the role of bacteria which, through their extracellular polymeric substances (EPS or biofilm), would act as primary nucleation centers for the oxidization and adsorption of metal ions promoting the formation of amorphous precursor phases that, later, precipitate as Fe–Mn oxy-hydroxides (e.g., Ehrlich 1975, 2002; Jansa et al. 1989; Lin et al. 1996; Han et al. 1997; Mamet and Préat 2006a; Wang et al. 2009; Reolid 2011; Lozano and Rossi 2012; Polgári et al. 2012; Rajabzadeh et al. 2017; Jiang et al. 2020). From this point of view, the petrographic observations of Fornazzo Fe–Mn deposits allowed us to distinguish arborescent and knobby texture in dendritic samples of diagenetic origin from laminated with internal digitate microstructure in Fe–Mn crusts formed by hydrogenetic precipitation (Figs. 4, 5 and 6). In this latter, microstuctures evidenced in Fig. 6 are very similar to those found by Reolid and Nieto (2010) in Jurassic Fe–Mn hardground from the Betic Cordillera (SE Spain). The authors, assigned the filaments to multicellular hyphae forming a fungal mycelium and preserved by Fe–Mn oxy-hydroxides, while ascribed the coccoid-shaped forms to cyanobacteria, not excluding other

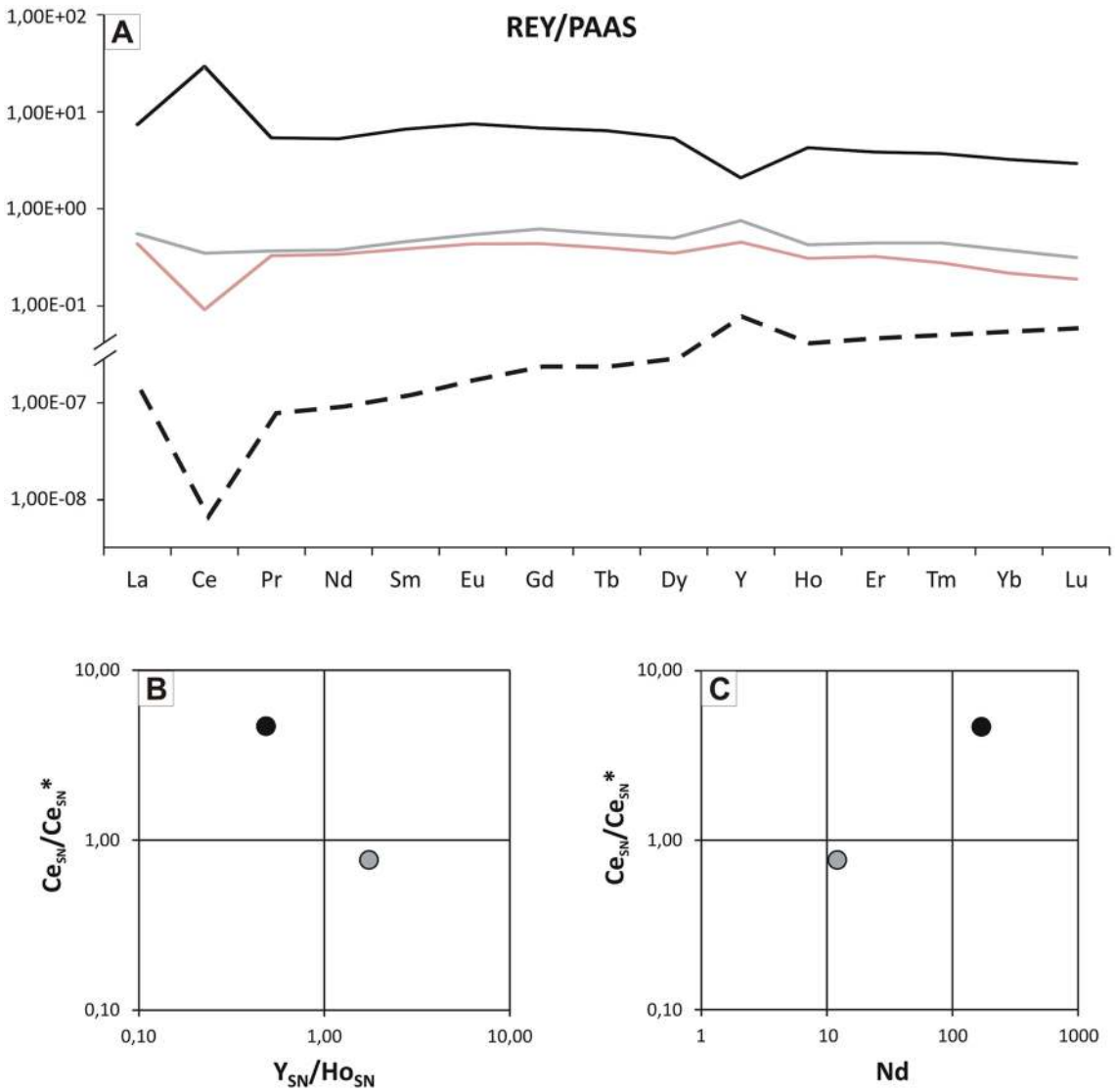

Fig. 9 **a** PAAS normalized REY spider diagram for the Fornazzo samples; dotted line is the typical deep seawater composition from Bao et al. 2008; PAAS from McLennan (1989). **b,c** Cross-plots of samples representing dendrite and Fe–Mn crust on graphs of $Ce_{SN}/Ce_{SN}*$ vs Y_{SN}/Ho_{SN} ratios and $Ce_{SN}/Ce_{SN}*$ vs Nd concentration (after Bau et al. 2014). Colors as in Fig. 7

possible types of eubacteria related to Fe and Mn oxidation. Filamentous microstructures, evoking hyphae, should point out for the authigenic minerals precipitation as consequence of microorganisms secretion of an iron chelating compound (siderophores), which could trap and transfer Fe^{3+} into the cell interior (Lewin 1984; Reolid and Nieto 2010). In this view, siderophores directly scavenge ferric iron promoting the biofilm formation which serve as a nucleation site for the mineral deposition. As for manganese, the binding of Mn chelates to cell-surface-associated Mn oxidase would activate the Mn^{2+} oxidation to Mn^{3+}, and then to Mn^{4+} (Brouwers et al. 2000; Toner et al. 2005; Zhang et al. 2015). The latters may precipitate as Mn-oxide layers onto the EPS (Zhang et al. 2015). Likewise, biofilms may produce a geochemical gradient that trap any suitable ions available in the proximity (e.g., Ni^{2+}, Co^{2+}, Cu^{2+}, Zn^{2+}), producing enrichments in these elements (Jiang et al. 2019).

The pelagic swells of the Trapanese platform, at the Middle Jurassic time, were favourable places for microbially mediated authigenesis due to: a) the sediment-starved conditions, and b) the injection in seawater of Fe, Mn, trace elements and REE, related to the incipient volcanic processes recorded in the Sicilian–Maghrebian realm. In fact, even if no geochemical signal indicates direct hydrothermal contribution to the Fe–Mn crusts, fragments of trachytic microtexture and felspar macro-crystals have been documented in the basal Rosso Ammonitico bed from others sections of the Trapanese domain, testifying a Middle−Upper Jurassic

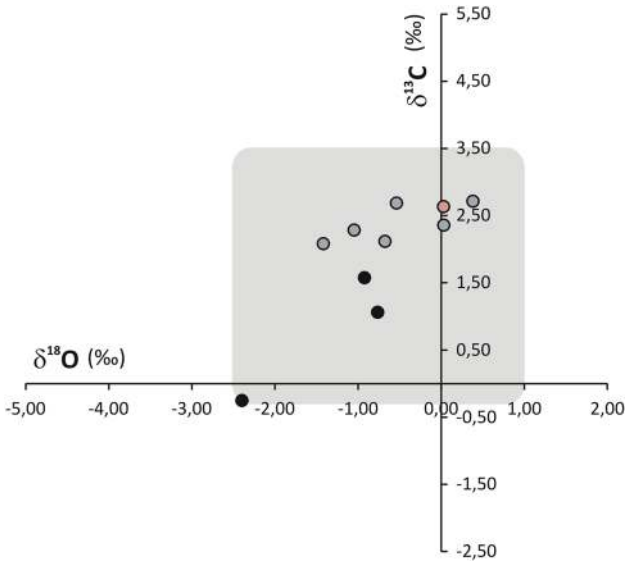

Fig. 10 $\delta^{13}C$ versus $\delta^{18}O$ cross-plot of the Fornazzo samples; grey area is the general field of the Jurassic marine carbonates from Veizer et al. (1999). Colors as in Fig. 7

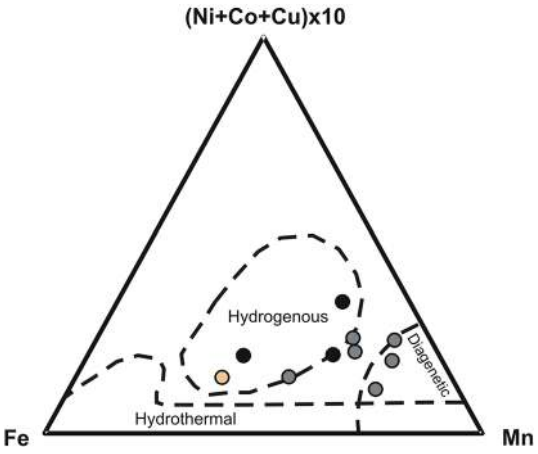

Fig. 11 Distribution of the studied samples in the ternary diagram of Fe–Mn-(Co + Ni + Cu) × 10 (after Toth 1980, Bonatti et al. 1972 and Hein et al. 1994). Colors as in Fig. 7

rift-related volcanic activity (Wendt 1963; Jenkyns and Torrens 1969; Jenkyns 1970a).

As for the arborescent microstructures in the early diagenetic dendritic samples (Figs. 4 and 5), they are associated to *Frutexites* shrubs, typically described in relation to crusts of Fe–Mn oxy-hydroxides (Böhm and Brachert 1993; Mamet and Préat 2006b; Cavalazzi et al. 2007). They grew within the already deposited sediment and are typically constituted by manganese that, as a highly mobile element, can be remobilized from crusts into younger sediments. In this context it is believed to be fundamental the role of specific Mn(IV)-reducing and Mn(II)-oxidizing bacteria biologically driving a closed Mn cycle (Blöthe et al. 2015). In particular, the origin of *Frutexites* was originally assigned to cyanobacteria (Maslov 1960; Szulczewski 1963) and to other phototrophic microbes (Myrow and Coniglio 1991). The involvement of chemosynthetic microorganisms has been consequently postulated to explain the formation of *Frutexites* structures in deep marine, aphotic environment, also ascribed to the Jurassic Fe–Mn *Frutexites* (Böhm and Brachert 1993; Préat et al. 2000; Reitner et al. 2000; Allouc and Harmelin 2001; Mamet and Préat 2003; Mišík and Aubrecht 2004; Reolid and Nieto 2010; Reolid 2011). As for the Fornazzo samples, microstructures of bacterial origin are not identified in the Mn-rich dendrites. It may be supposed that such components were obliterated during diagenetic growth of the dendrites, according to Dahanayake and Krumbein (1986) the bacterial mineralization can become undetectable due to iron encrustation. Microbial origin may be supported by the well-preserved micro-columnar/digitate structures, produced by the overlapping of "half-moon" constructions and commonly associated to microbial activity (e.g.,Mišík and Aubrecht 2004; Lozano and Rossi 2012; Polgári et al. 2012; Guido et al. 2016; Heim et al. 2017). Moreover, authigenic precipitation of carbonate-fluorapatite, typically ascribed to bacterial mediated processes in similar fluctuating redox conditions (O'Brien et al. 1981; Van Cappellen and Berner 1991; Sanchéz-Navas and Martín-Algarra 2001; Sannigrahi and Ingall 2005; Reolid and Nieto 2010), gives strength to this hypothesis.

Depositional environment

Coeval condensed levels and stratigraphic gaps characterized by similar ferromanganese deposits are widespread in the Western Tethyan Realm from the Trento Plateau (Winterer and Bosellini 1981; Clari et al. 1995; Martire 1996) to the Julian Alps (Šmuc and Rožic 2010) or Western Carpathians (Rojkovič et al. 2003) but also in a number of pelagic plateaus in the Apennines (e.g., Santantonio et al. 1996) and are interpreted as formed during a transgressive phase (Corbin et al. 2000). In particular, following these latter authors, the massive accumulation of Fe and Mn in the Late Callovian−Early Oxfordian interval should be also connected with intense syn-sedimentary tectonic activity corresponding to the start of the spreading in the western part of the Tethys Ocean. As for the Monte Inici area, the incipient volcanic process was likely responsible of the injection in seawater of Fe, Mn, trace elements and REE, but the Fe–Mn crusts and mineralizations are found to be hydrogenetic/diageneic in origin. The hydrogenetic laminated crusts were precipitated directly from seawater with an estimated growth rate of 8.5 mm/Myr in average. Since the maximum measured thickness was of 3 cm it is possible to estimate a time of deposition of ~ 3.5 ± 1 Myr. Given

that in the Fornazzo section the first age above the level of Fe–Mn concretions is middle Oxfordian (~ 159 Ma), the estimated time span should be compatible with the growth of the crusts during the stratigraphic gap between the top of the condensed "level 1" (early/middle Callovian; ~ 165 Ma) and the overlying pelagic limestone of the RAI (Fig. 1d). In this view, the spectacular Fe–Mn deposition should be the expression of one of the repeated satellite crusts formed above what Di Stefano and Mindszenty (2000) defined the "principal Fe–Mn-encrusted rockground" capping the Inici Fm. The roughly similarity of the deposition environment between the over- and underlying deposits gives indication that the crusts growth occurred in a system characterized only by limited variations of the environmental parameters and allows to define them as hardground (sensu Clari et al. 1995). The strong reduction in the rate of carbonate sedimentation contributed to the concentrations of metals precipitated as colloidal oxy-hydroxides from the oxygenated seawater. Since the only inorganic precipitation mechanisms are thought to be insufficient for the accumulation of significant thicknesses of Fe–Mn crusts, processes of microbial catalyzation operated to produce an efficient precipitation of Fe–Mn oxy-hydroxides. The documented coexistence of chemosynthetic fungi and photosynthetic cyanobacteria in Fe–Mn crusts testifies a palaeobathymetry compatible with the deep euphotic zone.

As for the reduction of carbonate deposition, excluding the subaerial exposition as testified by isotopic data, and the dissolution of the carbonate linked to the CCD proximity, the most plausible scenario accounts for an increased current activity that prevented the sediment accumulation or swept the bottom carrying away the already deposited oozes (Clari et al. 1995 and references therein). Referring to the complex system of small basins, swells and tilted block slopes, like proposed by Bernoulli and Jenkyns (1974), the Fe–Mn crusts from the Fornazzo section would precipitate during a transgressive phase on the more elevated area of a structural high characterized by strong current activity (Fig. 12).

Afterwards, during the early diagenesis, fluctuating redox conditions in the porewaters promoted the remobilization of Mn and other redox-sensitive elements. Their diffusion upwards in the sediments produced the growth of Mn-rich dendrites inside the freshly deposited carbonate. The consistency of the microbial community associated with the *Frutexites* to a scarce light availability gives indication of a variation in the paleobathymetry towards a deep marine, aphotic environment which probably promoted a restart in the carbonate sedimentation with the deposition of the overlying portion of RAI.

Conclusions

Results from the study on the Middle−Upper Jurassic Fe–Mn crusts and mineralizations from Fornazzo section (north-western Sicily) can be summarized as follows:

1. Macroscopic observations and mineralogical analyses allow to recognize two main typologies of Fe–Mn deposits: (i) Fe–Mn crusts, characterized by parallel dense lamination and with averagely high content in hematite and todorokite, and (ii) dendrites in limestones showing columnar or dome structure and prevalence in pyrolusite sometimes associated with carbonato-fluorapatite. For both of them, isotopic composition, in the range of Jurassic marine carbonates, gives evidence of submarine deposition.
2. Geochemical proxies, in particular Mn/Fe ratio and Co, Ni and Cu concentrations as well as the distribution of rare earths and Y, allow to discriminate a hydrogenetic origin for the Fe–Mn crusts and a prevalent early diagenetic origin for the dendrites related to a fluctuation in the porewaters redox conditions.
3. The cobalt concentration allows estimate average growth rates of 8.5 and 315 mm/Myr for the hydrogenous crusts and early diagenetic mineralizations, respectively. On

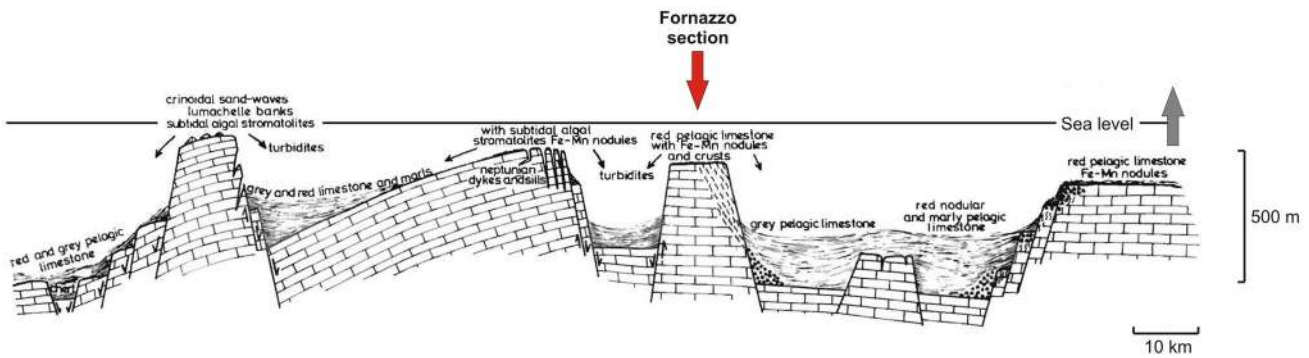

Fig. 12 Paleogeographic generalized scheme of southern continental margin of Tethys during Jurassic time (modified by Bernoulli and Jenkyns 1974); red arrow: depositional setting of the Fornazzo section during the Fe–Mn crusts growth

this base, a time span of ~ 3.5 ± 1 Myr was calculated for the growth of the hydrogenetic crusts, compatible with the stratigraphic gap above the Bathonian/Callovian condensed level of the Rosso Ammonitico and associated to the reduction in the carbonate sedimentation rate.

4. The contribution of microorganism activity in the precipitation of Fe–Mn oxy-hydroxides is documented in the Fe–Mn crusts with microstructures attributable to fungal mycelium and cyanobacteria, while have not been recognized in the dendrites probabily due to incipient recrystallization during diagenesis. Nevertheless, indication of the microbial influence is testified by the well-preserved micro-columnar/digitate structures, produced by the overlapping of "half-moon" constructions related to the well-know *Frutexites* structure. The different bacterial communities associated to Fe–Mn crusts and dendrites allow to suppose a deepening of the deposition environment also related to a restart in the carbonate sedimentation with the deposition of the overlying portion of RAI.

Acknowledgements Thanks are due to Rob Hoffman (Activation Laboratories Ltd—Canada) for useful suggestions relative to the appropriate analytical method to use for the elements determination and Franco Furnari for his help during the SEM observations. The authors would like to thank Luca Martire and Pietro Di Stefano for the constructive discussions about the local stratigraphy and Alberto Sciortino for reviewing the text's English. The authors are also indebted to Hans-Juergen Gawlick and the other anonymous reviewer for their valuable comments that greatly improved the manuscript. Financial support was provided by Ministero dell'Istruzione, dell'Univeristà e della Ricerca (ATE-EX60% 2012) grants to G. Scopelliti.

Funding Open access funding provided by Università degli Studi di Palermo within the CRUI-CARE Agreement.

References

Abad I, Reolid M, Jiménez-Millàn J (2010) Geochemistry and Mineralogy of Jurassic manganese crust from Jbel Moussa Group (Rifian Domain, Morocco): hydrothermal origin. Macla 13:33–34

Abouchami W, Galer SJG, Koschinsky A (1999) Pb and Nd isotopes in NE Atlantic Fe–Mn crusts: proxies for trace metal paleosources and paleocean circulation. Geochim Cosmochim Acta 63:1489–1505

Allouc J, Harmelin JG (2001) Mn-Fe deposits in shallow cryptic marine environment: examples in northwestern Mediterranean submarine caves. Bull Soc Géol Fr 172:765–778

Arkell WJ (1956) Jurassic geology of the world. Hafner Publishing Company, New York

Astakhova NV, Sattarova VV (2012) The REE species and their distribution in ferromanganese crusts in the Sea of Japan. Russ Geol Geophys 53:649–656

Atkins AL, Shaw S, Peacock CL (2016) Release of Ni from birnessite during transformation of birnessite to todorokite: Implications for Ni cycling in marine sediments. Geochim Cosmochim Acta 189:158–183

Ballarini L, Massari F, Nardi S, Scudeler Baccelle L (1994) Amino acids in the pelagic stromatolites of the rosso ammonitico veronese formation (Middle-Upper Jurassic, Southern Alps, Italy). In: Bertrand-Sarfati J, Monty C (eds) Phanerozoic stromatolites II. Kluwer Academic Publishers, Amsterdam, pp 279–294

Bao SX, Zhou HY, Peng XT, Ji FW, Yao HQ (2008) Geochemistry of REE and yttrium in hydrothermal fluids from the Endeavour segment, Juan de Fuca Ridge. Geochem J 42:359–370

Bau M (1996) Controls on the fractionation of isovalent trace elements in magmatic and aqueous systems: evidence from Y/Ho, Zr/Hf, and lanthanide tetrad effect. Contrib Mineral Petr 123:323–333

Bau M (1999) Scavenging of dissolved yttrium and rare earths by precipitating iron oxyhydroxide: experimental evidence for Ce oxidation, Y-Ho fractionation, and lanthanide tetrad effect. Geochim Cosmochim Acta 63:67–77

Bau M, Dulski P (1999) Comparing yttrium and rare earths in hydrothermal fluids from the Mid-Atlantic ridge: implications for Y and REE behaviour during near-vent mixing and for the Y/Ho ratio of Proterozoic seawater. Chem Geol 155:77–90

Bau M, Koschinsky A (2009) Oxidative scavenging of cerium on hydrous Fe oxide: evidence from the distribution of rare earth elements and yttrium between Fe oxides and Mn oxides in hydrogenetic ferromanganese crusts. Geochem J 43:37–47

Bau M, Dulski P, Möller P (1995) Yttrium and holmium in South Pacific seawater: vertical distribution and possible fractionation mechanisms. Chem Erde 55:1–15

Bau M, Schmidt K, Koschinsky A, Hein J, Kuhn T, Usui A (2014) Discriminating between different genetic types of marine ferromanganese crusts and nodules based on rare earth elements and yttrium. Chem Geol 381:1–9

Bayon G, German CR, Burton KW, Nesbitt RW, Rogers N (2004) Sedimentary Fe–Mn oxyhydroxides as paleoceanographic archives and the role of aeolian flux in regulating oceanic dissolved REE. Earth Planet Sc Lett 224:477–492

Beccaro P (2007) Radiolarian correlation of Jurassic siliceous successions of the Rosso Ammonitico Formation in the Southern Alps and Western Sicily (Italy). In: Baumgartner PO, Aitchison JC, De Wever P, Jackett SJ (eds) Radiolaria. Eclogae geol helv suppl 2. Birkhäuser, Basel

Bernoulli D, Jenkyns HC (1974) Alpine, Mediterranean, and central Atlantic Mesozoic facies in relation to the Early evolution of Tethys. In: Dott RH, Shaver RH (eds). Modern and Ancient Geosynclinal Sedimentation. Spec Publ Soc Econ Paleont Miner, Tulsa 19:129–160

Blöthe M, Wegorzewski A, Müller C, Simon F, Kuhn T, Schippers A (2015) Manganese-cycling microbial communities inside deep-sea manganese nodules. Environ Sci Technol 49:7692–7700

Bogdanov YA, Bogdanova OY, Dubinin AV, Gorand A, Gorshkov AI, Gurvich EG, Isaeva AB, Ivanov GV, Jansa LF, Monaco A (1995) Composition of ferromanganese crusts and nodules at northwest Pacific guyots and geologic and paleoceanographic considerations. In: Haggerty JA, Premoli Silva I, Rack FR, McNutt MK

(eds). Proceedings of the Ocean Drilling Program: Scientific Results 144, p 1059 (Ocean Drilling Program, College Station, TX)

Böhm F, Brachert TC (1993) Deep-water stromatolites and Frutexites Maslov from the Early and Middle Jurassic of S-Germany and Austria. Facies 28:145–168

Bolton BR, Both R, Exon NF, Hamilton TF, Ostwald J, Smith JD (1988) Geochemistry and mineralogy of seafloor hydrothermal and hydrogenetic Mn oxide deposits from the Manus Basin and Bismark Archipelago region of the southwest Pacific Ocean. Mar Geol 85:65–87

Bonatti E, Kraemer T, Rydell H (1972) Classification and genesis of submarine iron-manganese deposits. In: Horn DR (Ed.). Ferromanganese deposits on the ocean floor. Washington. pp 149−166

Brouwers GJ, Vijgenboom E, Corstjens PLAM, Vrind JPM, Joung EW (2000) Bacterial Mn^{2+} oxidizing systems and multicopper oxidases: an overview of mechanism and functions. Geomicrobiol J 17:1–24

Catalano R, D'Argenio B, Gregor BC, Nairn AEM, Nardi G (1981a) A paleomagnetic study of the Ammonitico Rosso of Western Sicily. In: Rosso Ammonitico Symposium Proceedings. Tecnoscienza Eds, Rome. pp 77−89

Catalano R, Abate B, Renda P (1981b) Carta geologica dei Monti di Palermo. Scala 1: 50.000. S.G.S., Roma

Catalano R, Di Stefano P, Sulli A, Vitale FP (1996) Paleogeography and structure of the central Mediterranean: Sicily and its offshore area. Tectonophysics 260:291–323

Cavalazzi B, Barbieri R, Ori GG (2007) Chemosynthetic microbialites in the Devonian carbonate mounds of Hamar Laghdad (Anti-Atlas, Morocco). Sediment Geol 200:73–88

Cecca F, Savary B (2007) Palaeontological study of Middle Oxfordian-Early Kimmeridgian (Late Jurassic) ammonites from the Rosso Ammonitico of Monte Inici (north-western Sicily, Italy). Geodiversitas 29:507–548

Cecca F, Fourcade E, Azéma J (1992) The disappearance of the "Ammonitico Rosso." Palaeogeogr Palaeoclimatol Palaeoecol 99:55–70

Cecca F, Savary B, Bartolini A, Remane J, Cordey F (2001) The Middle Jurassic-Lower Cretaceous Rosso Ammonitico succession of Monte Inici (Trapanese Domain, western Sicily); sedimentology, biostratigraphy and isotope stratigraphy. Bull Soc Géol Fr 172:647–659

Christ HA (1960) Beiträge zur Stratigraphie und Paläontologie des Malm von Westsizilien. Schweiz Palaeontol Abh 77:1–141

Clari PA, Dela Pierre F, Martire L (1995) Discontinuities in carbonate successions: identification, interpretation and classification of some Italian examples. Sediment Geol 100:97–121

Claude C, Suhr G, Hofmann AW, Koschinsky A (2005) U-Th chronology and paleoceanographic record in Fe–Mn crusts from the NE Atlantic over the last 700 ka. Geochim Cosmochim Acta 69:4845–4854

Corbin J-C, Person A, Iatzoura A, Ferré B, Renard M (2000) Manganese in Pelagic carbonates: indication of major Tectonic events during the geodynamic evolution of a passive continental margin (the Jurassic European Margin of the Tethys-Ligurian Sea). Palaeogeogr Palaeoclimatol Palaeoecol 156:123–138

Dahanayake K, Krumbein WE (1986) Microbial structures in oolitic iron formations. Miner Depos 21:85–94

de Baar HJW, Bacon PG, Brewer PG, Bruland KW (1985) Rare earth elements in the Pacific and Atlantic Oceans. Geochim Cosmochim Acta 49:1943–1959

Di Stefano P (2002) An introduction to the Jurassic Geology of Western Sicily. In: Santantonio M (ed) General field trip guidebook, VI international symposium on the jurassic system. Litografia Geda, Torino, pp 29–121

Di Stefano P, Mindszenty A (2000) Fe-Mn-encrusted "Kamenitza" and associated features in the Jurassic of Monte Kumeta (Sicily): subaerial and/or submarine dissolution? Sediment Geol 132:37–68

Di Stefano P, Galàcz A, Mallarino G, Mindszenty A, Vörös A (2002) Birth and early evolution of a Jurassic escarpment: Monte Kumeta, Western Sicily. Facies 46:273–298

Dromart G, Gaillard C, Jansa LF (1994) Deep-marine microbial structures in the Upper Jurassic of Western Tethys. In: Bertrand-Sarfati J, Monty C (eds) Phanerozoic stromatolites II. Kluwer Academic Publishers, Amsterdam, pp 295–318

Dunham RJ (1962) Classification of carbonate rocks according to depositional texture. In: Ham WE (Ed.). Classification of carbonate rocks, "A.A.P.G. Memoir" 1, pp 108–121

Edmonds HN, German CR (2004) Particle geochemistry in the rainbow hydrothermal plume, Mid-Atlantic Ridge. Geochim Cosmochim Acta 68:759–772

Ehrlich HL (1975) The formation of ores in the sedimentary environment of the deep sea with microbial participation: the case for ferromanganese concretions. Soil Sci 119:36–41

Ehrlich HL (2002) Geomicrobiology. Marcel Dekker, New York, p 768

Fleet AJ (1993) Hydrotermal and hydrogenous ferro-manganese deposits: do they form a continuum? The rare earth evidence. In: Rona PA, Boström K, Laubier L, Smith KL (eds) Hydrothermal processes at seafloor spreading centers. Plenum Press, New York, pp 535–555

Floridia GB (1931) Osservazioni geologiche sul M. Inici (Trapani). Boll Soc Geol Ital 50:87–112

Föllmi KB (2016) Sedimentary condensation. Earth-Sci Rev 152:143–180

Force ER, Cannon WF (1988) Depositional model for shallow-marine manganese deposits around black shale basins. Econ Geol 83:93–117

Frank M, O'Nions RK, Hein JR, Banakar VK (1999) 60 Myr records of major elements and Pb–Nd isotopes from hydrogenous ferromanganese crusts: reconstruction of seawater paleochemistry. Geochim Cosmochim Acta 63:1689–1708

Froelich PN, Arthur MA, Burnett WC, Deakin M, Hensley V, Jahnke R, Kaul L, Kim K-H, Roe K, Soutar A, Vathakanon C (1988) Early diagenesis of organic matter in Peru continental margin sediments: phosphorite precipitation. Mar Geol 80:309–343

Fürsich FT (1979) Genesis, environments, and ecology of Jurassic hardgrounds. N Jb Geol Paläont Abh 158:1–63

Fürsich FT, Oschmann W, Singh IB, Jaitly AK (1992) Hardgrounds, reworked concretion levels and condensed horizons in the Jurassic of western India: their significance for basin analysis. J Geol Soc 149:313–331

García-Ruiz JM, Otálora F, Sanchez-Navas A, Higes-Rolando FJ (1994) The formation of manganese dendrites as the mineral record of flow structures. In: Kruhl JH (ed) Fractals and dynamic systems in geoscience. Springer, Berlin, pp 307–318

Gemmellaro GG (1872–1882) Sopra alcune faune giuresi e liassiche della Sicilia. Atti Accad Lincei 12:451–472

German CR, Klinkhammer GP, Edmond JM, Mura A, Elderfield H (1990) Hydrothermal scavenging of rare-earth elements in the ocean. Nature 345:516–518

German CR, Colley S, Palmer MR, Khripounoff A, Klinkhammer GP (2002) Hydrothermal plume-particle fluxes at 13°N on the East Pacific Rise. Deep Sea Res Part I 49:1921–1940

Giacometti A, Ronchi P (2000) Early Lias Carbonate Platform: Facies and Diagenesis Analogies between the Calcare Massiccio (Umbro –Marchean Apennines) and the Inici Fm. (Sicily Channel). Mem Soc Geol It 55:271–278

Glasby GP (2000) Manganese: predominant role of nodules and crusts. In: Schultz HD, Zabel M (eds) Marine geochemistry. Springer, Heidelberg-New York, pp 35–372

Gugeberger O (1936) I cefalopodi del Lias Inferiore della Montagna del Casale in provincia di Palermo (Sicilia). Paleont It 36:135–213

Guido A, Rosso A, Sanfilippo R, Russo F, Mastandrea A (2016) Frutexites from microbial/metazoan bioconstructions of recent and Pleistocene marine caves (Sicily, Italy). Palaeogeogr Palaeoclimatol Palaeoecol 453:127–138

Gupta SM (1995) Palaeogene hardgrounds and associated intraclast lag deposits as the substrates of ferromanganese crusts and nuclei of nodules: Inferences of abyssal current in the Central Indian Ocean Basin. J Palaeontol Soc India 40:77–86

Han XQ, Shen HT, Chen JL, Qin JC, Zhang FS, Lin CY, Bian LZ (1997) Biogenesis and binary mineralization of organism and chemismus of polymetallic nodules from Pacific Ocean. Sci China 40:656–661

Han X, Jin X, Yang S, Fietzke J, Eisenhauer A (2003) Rhythmic growth of Pacific ferromanganese nodules and their Milankovitch climatic origin. Earth Planet Sc Lett 211:143–157

Harland WB, Armstrong RL, Cox AV, Craig LE, Smith AG, Smith DG (1990) A geologic time scale 1989. Cambridge University Press, Cambridge

Heim C, Quéric N-V, Ionescu D, Schäfer N, Reitner J (2017) Frutexites-like structures formed by iron oxidizing biofilms in the continental subsurface (Äspö Hard Rock Laboratory, Sweden). PLoS ONE 12:e0177542. https://doi.org/10.1371/journal.pone.0177542

Hein JR, Koski RA (1987) Bacterially mediated diagenetic origin for chert-hosted manganese deposits in the Franciscan Complex, California Coast Range. Geology 15:722–726

Hein JR, Hsueh-Wen Y, Gunn SH, Gibbs AE, Chung-ho W (1994) Composition and origin of hydrothermal ironstones from central Pacific seamounts. Geochim Cosmochim Acta 58:179–189

Hein JR, Koschinsky A, Halbach P, Manheim FT, Bau M, Kang JK, Lubick N (1997) Iron and manganese oxide mineralization in the Pacific. In: Nicholson K, Hein JR, Buhn B, Desgupta S (eds). Manganese Mineralization: geochemistry and mineralogy of terrestrial and marine deposits. Geol Soc Spec Publ 119:123−138

Hein JR, Koschinsky A, Bau M, Manheim FT, Kang J-K, Roberts L (2000) Co-rich ferromanganese crusts in the Pacific. In: Cronan DS (ed) Handbook of marine mineral deposits. CRC marine science series. CRC Press, Boca Raton, pp 239–279

Hein JR, Schulz MS, Dunham RE, Stern RJ, Bloomer SH (2008) Diffuse flow hydrothermal manganese mineralization along the active Mariana and southern Izu-Bonin arc system, western Pacific. J Geophys Res Solid Earth 113:B08S14

Hein JR, Conrad TA, Staudigel H (2010) Seamount mineral deposits, a source of rare metals for high technology industries. Oceanography 23:144–149

Hein JR, Mizell K, Koschinsky A, Conrad TA (2013) Deep-ocean mineral deposits as a source of critical metals for high- and green-technology applications: comparison with land-based resources. Ore Geol Rev 51:1–14

Hlawatsch S, Garbe-Schönberg CD, Lechtenberg F, Manceau A, Tamura N, Kulik DA, Kersten M (2002) Trace metal fluxes to ferromanganese nodules from the western Baltic Sea as a record for long-term environmental changes. Chem Geol 182:697–709

Jach R, Dudek T (2005) Origin of a Toarcian manganese carbonate/silicate deposit from the Krížna unit, Tatra Mountains, Poland. Chem Geol 224:136–152

Jansa LF, Pratt BR, Dromart G (1989) Deep water thrombolite mounds from the Upper Jurassic of offshore Nova Scotia. In: Geldsetzer HH, James NR, Tebbutt GE (eds). Reefs-Canada and Adjacent Area. Can Soc Petrol Geol Mem 13:725–735

Jarvis I, Burnett WC, Nathan Y, Almbaydin FSM, Attia AKM, Castro LN, Flicoteaux R, Hilmy ME, Husain V, Qutawnah AA, Serjani A, Zanin YN (1994) Phosphorite geochemistry: state-of-the-art and environmental concerns. Eclogae Geol Helv 87:643–700

Jenkyns HC (1967) Fossil manganese nodules from Sicily. Nature 216:673–674

Jenkyns HC (1970a) The Jurassic of western Sicily. In: Alvarez W, Gohrbandt HA (eds). Geology and History of Sicily. Petrol Expl Soc Lybia 245–254

Jenkyns HC (1970b) Fossil manganese nodules from the West Sicilian Jurassic. Eclogae Geol Helv 63:741–774

Jenkyns HC (1971) The genesis of condensed sequences in the Tethyan Jurassic. Lethaia 4:327–352

Jenkyns HC, Torrens HS (1969) Paleogeographic evolution of Jurassic seamounts in western Sicily. Preprint, Colloquium on Mediterranean Jurassic stratigraphy, Budapest, 1–19

Jiang X-D, Sun X-M, Guan Y (2019) Biogenic mineralization in the ferromanganese nodules and crusts from the South China Sea. J Asian Earth Sci 171:46–59

Jiang X-D, Gong J-L, Ren J-B, Liu Q-S, Zhang J, Chouc Y-M (2020) An interdependent relationship between microbial ecosystems and ferromanganese nodules from the Western Pacific Ocean. Sediment Geol 398:105588

Jiménez-Espinosa R, Jiménez-Millán J, Nieto L (1997) Factors controlling the genesis of Fe–Mn crusts in stratigraphic breaks of the eastern Betic Cordillera (SE Spain) deduced from numerical analysis of geological data. Sediment Geol 114:97–107

Koschinsky A, Halbach P (1995) Sequential leaching of marine ferromanganese precipitates: genetic implications. Geochim Cosmochim Acta 59:5113–5132

Koschinsky A, Halbach P, Hein JR, Mangini A (1996) Ferromanganese crusts as indicators for paleoceanographic events in the NE Atlantic. Geol Rundsch 85:567–576

Kuhn T, Bau M, Blum N, Halbach P (1998) Origin of negative Ce anomalies in mixed hydrothermal-hydrogenetic Fe-Mn crusts from the Central Indian Ridge. Earth Planet Sc Lett 163:207–220

Kuhn T, Wegorzewski AV, Rühlemann C, Vink A (2017) Composition, formation, and occurrence of polymetallic nodules. In: Sharma R (ed) Deep-sea mining. Springer, Cham, pp 23–63

Lamboy M (1990) Microstructure of a phosphatic crust from a Peruvian continental margin: phosphatized bacteria and associated phenomena. Oceanol Acta 13:439–451

Lewin R (1984) How microorganisms transport iron. Science 225:401–402

Lin CY, Bian LC, Zhang FS, Zhou LF, Chen JL, Shen HD (1996) Classification of the microbes and study of beaded ultramicrofossils in palagic manganese nodules. Chin Sci Bull 41:1364–1368

Loges A, Wagner T, Barth M, Bau M, Göb S, Markl G (2012) Negative Ce anomalies in Mn oxides: the role of Ce^{4+} mobility during water–mineral interaction. Geochim Cosmochim Acta 86:296–317

Lozano RP, Rossi C (2012) Exceptional preservation of Mn-oxidizing microbes in cave stromatolites (El Soplao, Spain). Sediment Geol 255(256):42–55

Lucas J, Prévôt L (1985) The syntesis of apatite by bacterial activity: mechanism. Sci Géol Mém 77:83–92

Mamet B, Préat A (2003) Sur l'origine bactérienne et fongique de la pigmentation de l'Ammonitico Rosso (Jurassique, région de Vérone, Italie du nord). Rev Micropaléontol 46:35–46

Mamet B, Préat A (2006a) Iron-bacterial mediation in Phanerozoic red limestones: state of the art. Sediment Geol 185:147–157

Mamet B, Prèat A (2006b) Jurassic microfacies, Rosso Ammonitico limestone, Subbetic Cordillera, Spain. Rev Esp Micropaleontol 38:219–228

Manheim FT (1986) Marine cobalt resources. Science 232:600–608

Manheim FT, Lane-Bostwick CM (1988) Cobalt in ferromanganese crusts as a monitor of hydrothermal discharge on the Pacific sea floor. Nature 335:59–62

Marino E, González FJ, Somoza L, Lunar R, Ortega L, Vázquez JT, Reyes J, Bellido E (2017) Strategic and rare elements in Cretaceous-Cenozoic cobalt-rich ferromanganese crusts from seamounts in the Canary Island Seamount Province (northeastern tropical Atlantic). Ore Geol Rev 87:41–61

Marino E, González FJ, Lunar R, Reyes J, Medialdea T, Castillo-Carrión M, Bellido E, Somoza L (2018) High-resolution analysis of critical minerals and elements in Fe–Mn crusts from the Canary Island Seamount Province (Atlantic Ocean). Minerals 8:285

Marino E, González FJ, Kuhn T, Madureira P, Wegorzewski AV, Mirao J, Medialdea T, Oeser M, Miguel C, Reyes J, Somoza L, Lunar R (2019) Hydrogenetic, diagenetic and hydrothermal processes forming ferromanganese crusts in the Canary Island Seamounts and their influence in the metal recovery rate with hydrometallurgical methods. Minerals 9:439

Martire L (1996) Stratigraphy, facies and synsedimentary tectonics in the Jurassic Rosso Ammonitico Veronese (Altopiano di Asiago, NE Italy). Facies 35:209–236

Martire L, Pavia G (2002) The trapanese domain. In: Santantonio M (ed) General field trip guidebook, vi international symposium on the jurassic system. Litografia Geda, Torino, pp 123–166

Maslov VP (1960) Stromatolites. Trudy Instituta Geologiceskich, Akademija Nauk, Moskva 41, pp. 188

McLennan SM (1989) Rare earth elements in sedimentary rocks. Influence of provenance and sedimentary processes. In: Lippin BR, McKay GA (eds). Geochemistry and Mineralogy of Rare Earth Elements. Rev Mineral 21:169–200

Mills RA, Wells DM, Roberts S (2001) Genesis of ferromanganese crusts from the TAG hydrothermal field. Chem Geol 176:283–293

Mišík M, Aubrecht R (2004) Some notes concerning mineralized hardgrounds (Jurassic and Cretaceous, Western Carpathians). Were all hardground always hard from the beginning? Slovak Geol Mag 10:183–202

Mitra A, Elderfield H, Greaves MJ (1994) Rare earth elements in submarine hydrothermal fluids and plumes from the Mid-Atlantic Ridge. Mar Chem 46:217–235

Myrow PM, Coniglio M (1991) Origin and diagenesis of cryptobiontic Frutexites in the Chapel Island Formation (Vendian to Early Cambrian) of southeast Newfoundland, Canada. Palaios 6:572–585

Nicholson K, Nayak VK, Nanda JK (1997) Manganese ores of the Ghoriajhor Monmunda area, Sundergarh District, Orissa, India: geochemical evidence for a mixed Mn source. Geol Soc Lond Spec Publ 119:117–121

Norrish K, Hutton JT (1969) An accurate X-ray spectrographic method for the analysis of a wide range of geological samples. Geochim Cosmochim Acta 33:431–453

O'Brien GW, Harris JR, Milnes AR, Veeh HH (1981) Bacterial origin of East Australian continental margin phosphorites. Nature 294:442–444

Ohta A, Ishii S, Sakakibara M, Mizuno A, Kawabe I (1999) Systematic correlation of the Ce anomaly with the Co/(Ni+Cu) ratio and Y fractionation from Ho in distinct types of Pacific deep-sea nodules. Geochem J 33:399–417

Okita PM, Maynard JB, Spiker EC, Force ER (1988) Isotopic evidence for organic matter oxidation by manganese reduction in the formation of stratiform manganese carbonate ore. Geochim Cosmochim Acta 52:2679–2685

O'Nions RK, Frank M, von Blanckenburg F, Ling H-F (1998) Secular variation of Nd and Pb isotopes in ferromanganese crusts from the Atlantic, Indian and Pacific Oceans. Earth Planet Sc Lett 155:15–28

Palmer TJ, Wilson MA (1990) Growth of ferruginous oncoliths in the Bajocian (Middle Jurassic) of Europe. Terra Nova 2:142–147

Patacca E, Scandone P, Giunta G, Liguori V (1979) Mesozoic Paleotectonic evolution of the Ragusa zone (Southeastern Sicily). Geol Rom 18:331–369

Pavia G, Lanza R, Lozar F, Martire L, Olóriz F, Zanella E (2004) Integrated stratigraphy from the Contrada Fornazzo section, Monte Inici, Western Sicily, Italy: proposed G.S.S.P. for the basal boundary of the Tithonian stage. Riv It Paleontol S 110:329–338

Piper DZ, Perkins RB (2004) A modern vs. permian black shale—the hydrography, primary productivity, and water-column chemistry of deposition. Chem Geol 206:177–197

Polgári M, Szabò-Drubina M, Szabò Z (2004) Theoretical model for Jurassic manganese mineralization in Central Europe, Urkùt, Hungary. Bull Geosci 79:53–61

Polgári M, Hein JR, Vigh T, Szabó-Drubina M, Fórizs I, Bíró LA, Müller A, Tóth AL (2012) Microbial processes and the origin of the Úrkút manganese deposit, Hungary. Ore Geol Rev 47:87–109

Préat A, Mamet B, De Ridder C, Boulvain F, Gillan D (2000) Iron bacterial and fungal mats, Bajocian stratotype (Mid-Jurassic, northern Normandy, France). Sediment Geol 137:107–126

Préat A, Mamet B, Di Stefano P, Martire L, Kolo K (2011) Microbially-induced Fe and Mn oxides in condensed pelagic sediments (Middle-Upper Jurassic, Western Sicily). Sediment Geol 237:179–188

Puteanus D, Halbach P (1988) Correlation of Co concentration and growth rate—A method for age determination of ferromanganese crusts. Chem Geol 69:73–85

Rajabzadeh MA, Haddada F, Polgári M, Fintor K, Walter H, Molnár Z, Gyollai I (2017) Investigation on the role of microorganisms in manganese mineralization from Abadeh-Tashk area, Fars Province, south western Iran by using petrographic and geochemical data. Ore Geol Rev 80:229–249

Reitner J, Thiel V, Zankl H, Michaelis W, Wörheide G, Gautret P (2000) Organic and biogeochemical patterns in cryptic microbialites. In: Riding RE, Awramik SM (eds) Microbial sediments. Springer, Berlin, pp 149–160

Ren XW, Liu JH, Shi XF, Yin JW (2011) Geochemistry of a marker of younger deposit of co-rich ferromanganese crust from Line Islands. Mar Geol Quatern Geol 31:41–46

Reolid M (2011) Palaeoenvironmental contexts for microbial communities from Fe-Mn crusts of middle-upper Jurassic hardgrounds (Betic-Rifian Cordillera). Rev Esp Paleontol 26:135–160

Reolid M, Nieto LM (2010) Jurassic Fe-Mn macro-oncoids from pelagic swells of the External Subbetic (Spain): evidence of microbial origin. Geol Acta 8:151–168

Riding R (2000) Microbial carbonates: the geological record of calcified bacterial-algal mats and biofilms. Sedimentology 47:179–214

Rodríguez-Martínez M, Heim CM, Quéric NV, Reitner J (2011) Frutexites. Encyclopedia of Earth sciences series. Springer, Netherlands, pp 396–401

Rojkovič I, Aubrecht R, Mišík M (2003) Mineral and chemical composition of manganese hardgrounds in Jurassic limestones of the Western Carpathians. Geol Carpath 54:317–328

Rona PA (2003) Resources of the sea floor. Science 299:673–674

Rona PA (2008) The changing vision of marine minerals. Ore Geol Rev 33:618–666

Sanchéz-Navas A, Martín-Algarra A (2001) Genesis of apatite in phosphate stromatolites. Eur J Min 13:361–376

Sannigrahi P, Ingall ED (2005) Polyphosphates as a source of enhanced P fluxes in marine sediments overlain by anoxic waters: evidence from ^{31}P NMR. Geochem T 6:52–59

Santantonio M, Galluzzo F, Gill G (1996) Anatomy and palaeobathymetry of a Jurassic pelagic carbonate platform/basin system. Rossa Mts., Central Apennines (Italy). Geol Implic Palaeopelagos 6:123–169

Schijf J, Marshall KS (2011) YREE sorption on hydrous ferric oxide in 0.5MNaCl solutions: a model extension. Mar Chem 123:32–43

Scopelliti G, Bellanca A, Neri R, Sabatino N (2010) Phosphogenesis in the Bonarelli Level from northwestern Sicily, Italy: petrographic evidence of microbial mediation and related REE behaviour. Cretac Res 31:237–248

Segl M, Mangini A, Bonani G, Hofmann HJ, Nessi M, Suter M, Wölfli W, Friedrich G, Plüger WL, Wiechowski A, Beer J (1984) ^{10}Be dating of a manganese crust from Central North Pacific and implications for oceanic paleocirculation. Nature 309:540–543

Sherrell RM, Field MP, Ravizza G (1999) Uptake and fractionation of rare earth elements on hydrothermal plume particles at 9°45′N, East Pacific Rise. Geochim Cosmochim Acta 63:1709–1722

Šmuc A, Rožič B (2010) The Jurassic Prehodavci Formation of the Julian Alps: easternmost outcrops of Rosso Ammonitico in the Southern Alps (NW Slovenia). Swiss J Geosci 103:241–255

Szulczewski M (1963) Stromatolites from the high-tatric Bathonian of the Tatra Mountains. Acta Geol Pol 13:125–141

Thiel GA (1925) Manganese precipitated by microorganisms. Econ Geol 20:301–310

Toner B, Fakra S, Villalobos M, Warwick T, Sposito G (2005) Spatially resolved characterization of biogenic manganese oxide production within a bacterial biofilm. Appl Environ Microbiol 71:1300–1310

Toth JR (1980) Deposition of submarine crusts rich in manganese and iron. Geol Soc Am Bull 91:44–54

Van Cappellen P, Berner RA (1991) Fluorapatite crystal growth from modified seawater solutions. Geochim Cosmochim Acta 55:1219–1234

Veizer J, Ala D, Azmy K, Bruckschen P, Buhl D, Bruhn F, Carden GAF, Diener A, Ebneth S, Godderis Y, Jasper T, Korte C, Pawellek F, Podlaha OG, Strauss H (1999) ^{87}Sr/^{86}Sr, δ^{13}C and δ^{18}O evolution of Phanerozoic seawater. Chem Geol 161:59–88

Wang S, Schlossmacher U, Natalio F, Schroder HC, Wolf SE, Tremel W, Muller WEG (2009) Evidence for biogenic processes during formation of ferromanganese crusts from the Pacific Ocean: implications of biologically induced mineralization. Micron 40:526–535

Wang G, Jansa L, Chu F, Zou C, Sun G (2015) Composition and origin of ferromanganese crusts from Equatorial Western Pacific Seamounts. J Ocean U China 14:217–227

Wendt J (1963) Stratigraphisch–paläeontologische Untersuchungen im Dogger Westsizilien. Boll Soc Paleontol It 2:57–145

Wendt J (1969) Die stratigraphisch–paläogeographische Entwicklung des Jura in Westsizilien. Geol Rundsch 58:735–755

Wendt J (2017) A unique fossil record from neptunian sills: the world's most extreme example of stratigraphic condensation (Jurassic, western Sicily). Acta Geol Pol 67:163–199

Winterer EL, Bosellini A (1981) Subsidence and sedimentation on Jurassic Passive Continental Margin, Southern Alps, Italy. AAPG Bull 65:394–421

Zhang Z, Zhang ZM, Chen H, Liu J, Liu C, Ni H, Zhao CS, Ali M, Liu F, Li L (2015) Surface Mn(II) oxidation actuated by a multicopper oxidase in a soil bacterium leads to the formation of manganese oxide minerals. Sci Rep 5:10895